Walking technicolor signatures at hadron colliders

Kenneth Lane and M. V. Ramana
Physics Department, Boston University, Boston, Massachusetts 02215
(Received 3 May 1991)

Aspects of the dynamics of walking technicolor models are expected to have important consequences for technihadron production at hadron colliders. Hard-mass enhancements characteristic of walking technicolor raise technipion (π_T) masses relative to technirho (ρ_T) masses so that the decays $\rho_T \to \pi_T\pi_T$ are either suppressed or forbidden altogether. Thus, ρ_T can be unusually narrow with unconventional decay modes. Large weak isospin breaking in U- and D-technifermion masses (required for t-b splitting) leads to neutral ρ_T and π_T that are ideally mixed. Finally, multiscale models of walking technicolor in which the light-scale technifermions carry ordinary SU(3) color can have color-octet ρ_T's which are produced strongly in parton-parton collisions and are within reach of the Fermilab Tevatron. These would appear as narrow, well-separated $\rho_{\bar{D}D}$ and $\rho_{\bar{U}U}$ resonances in dijet production or in $\pi_T\pi_T$ production with a limited number of final states. These expectations are illustrated in a multiscale model containing both techniquarks and technileptons at the light scale. Depending on assumptions that determine the fundamental chiral-symmetry-breaking mass parameters of the model, we find two generic phenomenologies: (A) $\rho_{\bar{D}D}$ with a mass of 200–250 GeV decaying exclusively to dijets and $\rho_{\bar{U}U}$ in the mass range 350–550 GeV decaying to a few $\pi_T\pi_T$ combinations; (B) $\rho_{\bar{D}D}$ with a mass of 375–425 GeV and $\rho_{\bar{U}U}$ in the mass range 500–700 GeV both decaying to a few $\pi_T\pi_T$ modes. The $\rho_{\bar{D}D} \to$ dijet signal of case A is large at all colliders and can be sought now at the Tevatron. The $\pi_T\pi_T$ production rates in both cases are of ~ 10 pb at the Tevatron and ~ 10 nb at the Superconducting Super Collider (SSC). The technipions can be sought in the next high-luminosity run of the Tevatron and may be excludable if backgrounds are not too severe. Experiments at the SSC certainly should be able to determine whether they exist.

I. INTRODUCTION

Most of the experimental signatures for technicolor have long been regarded as very difficult to detect, even at very-high-energy colliders such as the Superconducting Super Collider (SSC) and CERN Large Hadron Collider (LHC) [1,2]. In the minimal model, with one technifermion doublet, the only signals are modest enhancements in W^+W^- and $W^\pm Z^0$ production near an invariant mass of 1.5–2 TeV. These processes have small $[O(\alpha^2)]$ cross sections and their observability is beset by the well-known difficulties of reconstructing weak-boson invariant masses with reasonable efficiencies. Nonminimal technicolor (TC) models have a rich spectrum of technirho vector mesons (ρ_T) and technipion (π_T) states into which they may decay. The ρ_T have been expected either to be very heavy and produced with small cross sections or to be very broad and nearly indistinguishable as resonances in π_T-pair production. Moreover, the π_T are expected to decay to heavy-fermion pairs, and these can be difficult final states to isolate and reconstruct.

The purpose of this paper is to show that these gloomy prospects may be considerably brightened in models of walking technicolor [3]. We shall argue that the peculiar dynamics of walking technicolor results in ρ_T which are relatively narrow and have decay modes more amenable to detection. If these ρ_T are ordinary color octets, they will have large production rates in hadron colliders, typically of $O(\alpha_{\rm QCD}^2)$. And, if walking technicolor is implemented by having several scales of technifermion chiral-symmetry breaking, the hadrons associated with the lightest scale may be within reach of the Fermilab Tevatron collider. These expectations will be supported by calculations in a detailed (although ultimately unrealistic) model of walking technicolor.

Walking technicolor has been advocated as a solution to the problem of large flavor-changing neutral-current interactions in extended technicolor (ETC) theories of quark and lepton mass generation [4,5]. Walking theories are characterized by a gauge coupling $\alpha_{\rm TC}$ that evolves very slowly over a large range of momentum above the energy scale $\Lambda_{\rm TC}$ at which technifermion chiral symmetries are spontaneously broken. Consequently, the anomalous dimension γ_m of the technifermion bilinear $\bar{T}T$ remains close to unity over this momentum range. This enhances significantly the condensate $\langle \bar{T}T \rangle_{\rm ETC}$ and hence, the "hard" masses of technifermions, quarks, and leptons for a fixed ETC energy scale $M_{\rm ETC}$. Thus, $M_{\rm ETC}$ may be raised to several hundred TeV so that ETC-generated flavor-changing neutral currents are rendered harmless [5].

Hard-mass enhancement is the first feature of walking technicolor dynamics that has an impact on its phenomenology. It implies that the masses of π_T may be so large that the decays $\rho_T \to \pi_T\pi_T$ preferred by selection rules are either suppressed kinematically or forbidden altogether [6]. The ρ_T are then likely to appear as narrow, distinct resonances in hadron collisions. Only the production of ordinary SU(3)-color singlet ρ_T mesons was considered in [6]. These ρ_T may have useful, anomalously

large branching ratios to identifiable final states involving a $W^{\pm}$ or Z^0 boson plus a pair of hadron jets or leptons from π_T decay. Unfortunately, they are produced at small $[O(\alpha^2)]$ rates via their electroweak couplings to quarks. In this paper, therefore, we concentrate on color-octet ρ_T's which are produced much more copiously in hadron collisions via their coupling to a single gluon. The suppression of their $\pi_T\pi_T$ decay modes implies that they may have appreciable branching ratios to quark-antiquark ($q\bar{q}$) and two-gluon ($\mathcal{G}\mathcal{G}$) final states and that they can appear as narrow ($\lesssim 10$ GeV) resonances in *ordinary dijet production.*

The second aspect of walking technicolor dynamics that dramatically affects its phenomenology is the large weak isospin breaking needed to produce the mass difference between t and b quarks [7]. This requires large mass splittings between up (U) and down (D) technifermions. Consequently, both color-octet and color-singlet ρ_T's are likely to appear as *well-separated, ideally mixed* ($\bar{U}U$ and $\bar{D}D$) narrow resonances in dijet production and/or π_T-pair production. This ideal mixing, together with π_T mass enhancement, sharply reduces the number of distinct final states in $\rho_T \to \pi_T\pi_T$ and may make the experimentalists' task of isolating these states easier.

Finally, multiscale technicolor models have been proposed as a way to implement a walking coupling [6]. In these models $\alpha_{\rm TC}$ runs slowly because there are many technifermions in fundamental representations of the TC gauge group *and* a few technifermions in higher-dimensional representations. The differing representations give rise to two or more scales Λ_i of technifermion chiral-symmetry breaking and corresponding mass scales of technihadrons. There is some expectation that a sizable hierarchy will occur among these scales, depending on the relative dimensionalities of the representations [8]. The largest scale is set by the characteristic energy of electroweak symmetry breaking, $\Lambda_{\rm max} \lesssim 1$ TeV. Thus, if a large hierarchy occurs, the smallest scales will be so low that the corresponding ρ_T's, especially the colored ones produced with large cross sections, will be readily accessible at the Fermilab Tevatron collider as well as at the LHC and SSC. In this paper we investigate the phenomenology of such a multiscale hierarchy.

To summarize, in multiscale models of walking technicolor, we expect well-separated, low-mass $\rho_{\bar{D}D}$ and $\rho_{\bar{U}U}$ produced via $\bar{q}q$ and $\mathcal{G}\mathcal{G}$ collisions. Their $\pi_T\pi_T$ widths could be as small as a few tens of GeV and, if these channels are closed, they could be as narrow as a few GeV. A 200-GeV ρ_T decaying only to dijets with an $O(\alpha_{\rm QCD}^2)$ width of 5 GeV would have a partonic production cross section of $\sim \pi\alpha_{\rm QCD}^4/M_{\rho T}\Gamma_{\rho T} \sim 100$ pb. A 600-GeV ρ_T decaying to $\pi_T\pi_T$ with a width of 50 GeV would have a partonic rate of $\sim \pi\alpha_{\rm QCD}^2/M_{\rho T}\Gamma_{\rho T} \sim 400$ pb. Of course, these rates must be folded with the parton distribution functions. But it is clear that even Tevatron experiments can put very significant limits on the mass scales in walking technicolor models. We urge that the color-octet ρ_T be looked for as soon as possible, in both dijet and $\pi_T\pi_T$ production.

The rest of this paper is organized as follows. In Sec. II we present a multiscale model of walking technicolor that we will use to illustrate the masses and production rates of colored ρ_T and π_T technihadrons that can arise. The lightest technifermions in this model are an electroweak doublet of color-triplet "techniquarks" and N_L doublets of color-singlet "technileptons," all transforming as the fundamental representation of the TC gauge group SU($N_{\rm TC}$). We describe in some detail how the fundamental energy scales and technihadron masses are calculated, paying special attention to the questionable assumptions and peculiar difficulties calculations in such a model entail. Two methods of calculating the fundamental scales are presented. Both methods mainly derive from a naive scaling from QCD. They differ in whether the decay constants F_{π_T} of π_T do or do not scale with the dimensionality of the SU($N_{\rm TC}$) representation of their constituent technifermions.

The output of these methods are two rather different classes of ρ_T and π_T masses. The technihadrons are nearly ideally mixed in both cases, resulting in color-octet $\rho_{\bar{D}D}$ and $\rho_{\bar{U}U}$. We pick a "typical" representative set of technihadron masses from each class. In Set A, $M_{\rho_{\bar{D}D}} \simeq 225$ GeV and $M_{\rho_{\bar{U}U}} \simeq 465$ GeV. In Set B, $M_{\rho_{\bar{D}D}} \simeq 400$ GeV and $M_{\rho_{\bar{U}U}} \simeq 575$ GeV. The $\rho_{\bar{D}D}$ in Case A decays exclusively to dijets. We emphasize that the detailed values of the technihadron masses in these two sets are only representative of their class. Depending on various input parameters, there can be 25–100 GeV variations, especially in the masses of states containing one or two U techniquarks. These variations can make significant changes in production rates. Nevertheless, in both classes, many of the $\rho_T \to \pi_T\pi_T$ decay modes are closed, so that the ρ_T are quite narrow resonances with measurable cross sections at the Tevatron energy.

In Sec. III we show how the dijet invariant-mass distribution and the π_T-pair production cross section are modified to include two mixed color-octet ρ_T vector-meson resonances. Sections II and III may be skimmed by the reader willing to accept uncritically the input sets A and B of technihadron masses and the formulas for the relevant hadron collider cross sections.

In Sec. IV we calculate the dijet and $\pi_T\pi_T$ cross sections for the mass parameter sets A and B. These calculations are done for $\bar{p}p$ collisions at $\sqrt{s} = 630$ GeV ($S\bar{p}pS$) and 1800 GeV (Tevatron) and for pp collisions at $\sqrt{s} = 17$ TeV (LHC) and 40 TeV (SSC). For the Set-A parameters, we find the following.

(i) $\rho_{\bar{D}D}$ decays only into $\bar{q}q$ and $\mathcal{G}\mathcal{G}$ jets and is a prominent narrow ($\simeq 4$ GeV) resonance in dijet production at all the colliders. Excluding this resonance is limited only by a detector's jet energy resolution and it may possible to do this with data already taken by the Collider Detector at Fermilab (CDF) Collaboration at the Tevatron.

(ii) $\rho_{\bar{U}U}$ decays mainly to π_T pairs with a total width of about 20 GeV. According to the conventional wisdom, these technipions decay to a heavy quark-lepton pair or to a heavy $q\bar{q}$ pair. In these modes, the $\rho_{\bar{U}U}$ should be accessible at the Tevatron and certainly may be found at the SSC and LHC provided the backgrounds are not too

severe. These backgrounds need and deserve careful study. The $\rho_{\bar{U}U}$ has a branching ratio of about 25% to dijets, but with its relatively large mass and width, we doubt that it can be observed in these modes at any collider *unless* quark and gluon jets can be distinguished and the quark-jet sample enriched.

For the Set-B parameters, both $\rho_{\bar{D}D}$ and $\rho_{\bar{U}U}$ decay mainly to $\pi_T\pi_T$ and, modulo the backgrounds, should be observable in these modes at the Tevatron, LHC, and SSC. The width of the $\rho_{\bar{D}D}$ is about 40 GeV and that of the $\rho_{\bar{U}U}$ about 20 GeV. Thus, in this case, the $\rho_{\bar{D}D}$ is completely invisible in dijet production, and the $\rho_{\bar{U}U}$ very likely is too.

The technihadron masses and production rates that emerge from our calculations are in accord with our general expectations for any multiscale model of walking technicolor. By examining the consequences of two different schemes for estimating the fundamental energy scales of a particular model, we believe we present a reasonably broad spectrum of the experimental signatures possible in such models. Our basic message to experimentalists is that they should be prepared to look for signals in a variety of ways: dijets; multijets, probably involving heavy quarks; and two jets plus two leptons which may be τ's.

Finally, some of the details of the calculation of technifermion hard masses and π_T masses generated by the ETC interactions are presented in an Appendix.

II. A MULTISCALE MODEL OF WALKING TECHNICOLOR

In this section we present a model of walking technicolor which has three different species of technifermions, we describe the model's spectrum of low-lying technihadrons, and we outline the calculation of its fundamental energy scales and masses of relevant technihadrons.

A. The model and its technihadron spectrum

Walking technicolor models require a large number of technifermions in order that $\alpha_{\rm TC}$ runs slowly. These fermions may belong to the fundamental representation of the TC gauge group, to higher-dimensional representations, or to both, so-called multiscale models [6]. In any case, these models almost certainly contain technifermions which carry ordinary color-SU(3) quantum numbers and, hence, technihadrons which are colored and can be produced copiously in hadron colliders. To illustrate the more dramatic phenomenological consequences of walking technicolor, we consider in this paper a specific multiscale model. This model contains one doublet $\psi=(\psi_U,\psi_D)$ of color-singlet technifermions in the antisymmetric tensor representation of the TC gauge group $\mathrm{SU}(N_{\rm TC})$; one doublet of color-triplet techniquarks, $Q=(U,D)$; and N_L doublets of color-singlet technileptons, $L_m=(N_m,E_m), m=1,\ldots,N_L$. Q and L transform as the fundamental representation of $\mathrm{SU}(N_{\rm TC})$.

The model is based on the ETC gauge group

$$G_{\rm ETC}=\mathrm{SU}(N_{\rm ETC})_1\otimes\mathrm{SU}(N_{\rm ETC})_2\ ,$$
$$N_{\rm ETC}=N_{\rm TC}+3+N_L\ . \tag{2.1}$$

The ETC gauge couplings are g_1 and g_2. This group commutes with the $\mathrm{SU}(2)_{\rm EW}$ part of the electroweak gauge group, but not with its U(1) part (see [5]). All technifermions and ordinary light fermions are assigned to four irreducible representations of $\mathrm{SU}(N_{\rm ETC})_1\otimes\mathrm{SU}(N_{\rm ETC})_2$. With an obvious notation, $\mathcal{U}_L,\mathcal{D}_L,\mathcal{U}_R\in(\mathsf{A}_2,1)$ and $\mathcal{D}_R\in(1,\mathsf{A}_2)$, where A_2 is the antisymmetric second-rank tensor. At the energy scale M_A, $\mathrm{SU}(N_{\rm ETC})_1\otimes\mathrm{SU}(N_{\rm ETC})_2$ is assumed to be broken down to the diagonal subgroup $\mathrm{SU}(N_{\rm ETC})_{1+2}$. At the scale $M_V<M_A$, this group is further broken down to $\mathrm{SU}(N_{\rm TC})\otimes\mathrm{SU}(3)\otimes\mathrm{SU}(N_L)$. Since technicolor and color are unified at the ETC scale M_V, their couplings are given by $\alpha_{\rm TC}(M_V)=\alpha_{\rm QCD}(M_V)=\alpha_{\rm ETC}\equiv g_{\rm ETC}^2/4\pi$, where $g_{\rm ETC}=g_1g_2/\sqrt{g_1^2+g_2^2}$.

To reduce the number of free parameters in this model and keep our calculations tractable, technilepton flavor splitting is *not* included in the assumed pattern of gauge symmetry breakdown. Then, the technifermions can be classified according to $\mathrm{SU}(N_{\rm TC})\otimes\mathrm{SU}(3)\otimes\mathrm{SU}(N_L)\otimes\mathrm{SU}(2)$, where SU(2) is the isospin group which has $\mathrm{SU}(2)_{\rm EW}$ as its left-handed part. The technifermions are

$$T_{3\,L,R}\equiv\psi_{L,R}\in(\mathsf{A}_2,1,1,2)\ ,$$
$$T_{2\,L,R}\equiv Q_{L,R}\in(\mathsf{N}_{\rm TC},3,1,2)\ , \tag{2.2}$$
$$T_{1\,L,R}\equiv L_{L,R}\in(\mathsf{N}_{\rm TC},1,\mathsf{N}_L,2)\ .$$

The left-handed fields are $\mathrm{SU}(2)_{\rm EW}$ doublets, while the right-handed ones are $\mathrm{SU}(2)_{\rm EW}$ singlets. Note that ETC interactions explicitly break the right-handed part of SU(2), thereby splitting up and down technifermions.

This ETC model has several serious deficiencies: ETC gauge anomalies (to be canceled by unspecified fermions that effect ETC breaking?), too many quarks and leptons [9], and massive neutrinos. But the model has some useful features: the coupling $\alpha_{\rm TC}$ walks slowly to the ETC scale M_V. There are three scales Λ_i of technifermion chiral-symmetry breaking. And the ETC interactions are explicit enough to permit detailed estimates of technifermion and technihadron masses (when augmented by certain QCD-based rules of calculation).

At this point, we alert the reader to two important assumptions we shall make to calculate these masses. First, we shall assume that ETC interactions are not very important in driving the *spontaneous* breakdown of technifermion chiral symmetries. This means we shall assume the validity of chiral perturbation theory for calculating π_T masses, using broken ETC interactions in first order. A strong-ETC alternative has been proposed as a way to explain the apparently very heavy top quark [10]. At the end of this paper we shall briefly discuss how we expect strong-ETC interactions to modify our conclusions.

Our second assumption is that technifermion scales

and condensates, Λ_i and $\langle \bar{T}_i T_i \rangle (i=L,Q,\psi=1,2,3), \pi_T$ decay constants F_i, and the masses of ρ_T and their coupling to $\pi_T\pi_T$ may be estimated from the corresponding QCD parameters by naive scaling and large $N_{\rm TC}$ arguments. Since we have no direct experience with gauge theories where the coupling stays near the same large value for a wide range of momentum nor with higher-dimensional representations of the confining gauge group, it is not at all clear that QCD-based estimates are valid here.

In the neglect of ETC interactions, the technifermions in (2.2) enjoy a chiral flavor symmetry

$$\mathcal{G}_F = [\mathrm{SU}(2)\otimes\mathrm{SU}(2)]_\psi \otimes [\mathrm{SU}(2N_L+6)\otimes\mathrm{SU}(2N_L+6)]_{Q,L}\otimes \mathrm{U}_A(1)\ . \quad (2.3)$$

Here we are anticipating the fact that, although color SU(3) becomes asymptotically nonfree above the Q threshold, it is still weak enough to be neglected in enumerating approximate flavor symmetries. The $\mathrm{U}_A(1)$ symmetry in (2.3) is generated by the obvious $\mathrm{SU}(N_{\rm TC})$ anomaly-free combination of axial-U(1) ψ and Q,L currents. These chiral symmetries are spontaneously broken at the scales Λ_ψ, Λ_Q, and Λ_L to

$$\mathcal{S}_F = \mathrm{SU}(2)_\psi \otimes \mathrm{SU}(2N_L+6)_{Q,L}\ . \quad (2.4)$$

We shall soon define the Λ_i more precisely. It will turn out that $\Lambda_\psi > \Lambda_Q \cong \Lambda_L$. This symmetry breakdown results in $3+(2N_L+6)^2-1+1$ Goldstone bosons π_T. All but three of these, the longitudinal components of the $W^\pm$ and Z^0 bosons, acquire mass from the broken ETC interactions. From now on, we restrict our attention to those technipions which can be produced in QCD-mediated collisions of $\bar{q}q$ and $\mathcal{G}\mathcal{G}$.

In this multiscale model, the spectrum of low-lying technihadrons includes ρ_T and π_T, which are color-octet and color-singlet $\bar{Q}Q$ bound states, color-triplet $\bar{L}Q$ and $\bar{Q}L$ states, and color-singlet $\bar{L}L$ states [11]. We concentrate first on the electrically neutral color-octet ρ_8^I, since these are strongly produced in hadron collisions. There are two sets of such mesons, ρ_8^{0a} and ρ_8^{1a}, which transform as $(I,I_3)=(0,0)$ and (1,0) under SU(2), respectively. Here, $a=1,\ldots,8$ is an SU(3) index. There is a direct single-QCD-gluon coupling to ρ_8^{0a}, but none to ρ_8^{1a}. However, there is necessarily a mixing between ρ_8^{0a} and ρ_8^{1a} so that both may be produced in hadron collisions. ETC interactions break SU(2), splitting the "hard" masses m_U and m_D of the techniquarks U and D. This induces mixing in both the mass and width matrices of ρ_8^{0a} and ρ_8^{1a}. Their diagonal masses, given later in Eq. (2.26), are nearly equal. We shall find in model calculations that the widths of ρ_8^{0a} and ρ_8^{1a} also are comparable when calculated at the *same* mass. (The formulas for these widths are given in Table I below.) It follows that the states produced in hadron collisions are approximately the ideally mixed $\rho^a_{\bar{U}U}$ and $\rho^a_{\bar{D}D}$.

The spectrum of colored technipions into which ρ_8^I can decay will also be ideally mixed. These include two unit-charged color octets $\pi^a_{\bar{D}U}$ and $\pi^a_{\bar{U}D}$, two neutral octets $\pi^a_{\bar{U}U}$ and $\pi^a_{\bar{D}D}$, and $4N_L$ "leptoquark" color triplets $\pi_{\bar{N}U}, \pi_{\bar{N}D}, \pi_{\bar{E}U}, \pi_{\bar{E}D}$ plus their antiparticles. In addition, ρ_8^{1a} can decay to $\pi^a_{\bar{U}D}W^+$ and $\pi^a_{\bar{U}D}P_i^+$ $(i=1,2)$. In the limit $\Lambda_\psi \gg \Lambda_Q \cong \Lambda_L$, the longitudinal component of W^+ is mainly a $\bar{\psi}_D\psi_U$ state with small $\bar{D}U$ and $\bar{E}N$ pieces, while the orthogonal color-singlet, SU(2)-triplet states P_1^+ and P_2^+ are mainly $\bar{E}N$ and $\bar{D}U$, respectively [12]. The amplitudes and rates for the decays $\rho_8^I \to \pi_T\pi_T$ are listed in Table I. The amplitudes are computed in the SU(2)-isospin and $\mathrm{SU}(N_L)$-flavor-symmetry limits (also see [1]). The $\rho_8^I \to \pi_T\pi_T$ decay constant g_{ρ_T} is assumed to be scaled from the constant for $\rho\to\pi\pi$ in QCD according to

$$\alpha_{\rho_T} \equiv \frac{g^2_{\rho_T}}{4\pi} \cong 2.97\left[\frac{3}{N_{\rm TC}}\right]\ . \quad (2.5)$$

This is the first example of a QCD-based estimate that we should be wary of in a walking gauge theory.

B. The walking coupling and the mass scales

We now describe how a walking $\alpha_{\rm TC}$ is achieved in this class of multiscale models. Then we discuss how we determine the basic energies of the model: the ETC-

TABLE I. Amplitudes and widths for $\rho_T \to \pi_T\pi_T$. Amplitudes for $\rho_T^{Ia} \to \pi_T^B(k_1)\pi_T^C(k_2)$ are given by $ig_{\rho_T}C_I^{aBC}(k_1-k_2)\cdot\epsilon_{\rho_T}$ and the corresponding s-dependent widths by $\Gamma_{IJ} = g^2_{\rho_T}\tilde{\Gamma}_{IJ}k^3/s$. The unitary matrix mixing factors γ_W and γ_k $(k=1,2)$ give the $\bar{D}U$ content of W^+, P_1^+, and P_2^+. Note that $\sum_{\rm modes}\tilde{\Gamma}_{II} = 3+N_L$ and $\sum_{\rm modes}\tilde{\Gamma}_{01}=0$.

Decay	C_0^{aBC}	C_1^{aBC}	$\tilde{\Gamma}_{00}$	$\tilde{\Gamma}_{11}$	$\tilde{\Gamma}_{01}$
$\pi^b_{\bar{D}U}\pi^c_{\bar{U}D}$	$-if_{abc}$	$-d_{abc}$	$\frac{3}{2}$	$\frac{5}{6}$	0
$\pi^b_{\bar{U}U}\pi^c_{\bar{U}U}$	$-if_{abc}$	$-if_{abc}$	$\frac{3}{4}$	$\frac{3}{4}$	$\frac{3}{4}$
$\pi^b_{\bar{D}D}\pi^c_{\bar{D}D}$	$-if_{abc}$	if_{abc}	$\frac{3}{4}$	$\frac{3}{4}$	$-\frac{3}{4}$
$\pi^B_{\bar{N}U}\pi^C_{\bar{U}N}$	$(\frac{1}{2}\lambda^a)_{CB}$	$(\frac{1}{2}\lambda^a)_{CB}$	$\frac{1}{4}N_L$	$\frac{1}{4}N_L$	$\frac{1}{4}N_L$
$\pi^B_{\bar{E}U}\pi^C_{\bar{U}E}$	$(\frac{1}{2}\lambda^a)_{CB}$	$(\frac{1}{2}\lambda^a)_{CB}$	$\frac{1}{4}N_L$	$\frac{1}{4}N_L$	$\frac{1}{4}N_L$
$\pi^B_{\bar{N}D}\pi^C_{\bar{D}N}$	$(\frac{1}{2}\lambda^a)_{CB}$	$-(\frac{1}{2}\lambda^a)_{CB}$	$\frac{1}{4}N_L$	$\frac{1}{4}N_L$	$-\frac{1}{4}N_L$
$\pi^B_{\bar{E}D}\pi^C_{\bar{D}E}$	$(\frac{1}{2}\lambda^a)_{CB}$	$-(\frac{1}{2}\lambda^a)_{CB}$	$\frac{1}{4}N_L$	$\frac{1}{4}N_L$	$-\frac{1}{4}N_L$
$W^+\pi^b_{\bar{D}U}$	0	$-(1/\sqrt{3})\gamma_W\delta_{ab}$	0	$\frac{1}{3}\gamma_W^2$	0
$P_k^+\pi^b_{\bar{D}U}$	0	$-(1/\sqrt{3})\gamma_k\delta_{ab}$	0	$\frac{1}{3}\gamma_k^2$	0

breaking scales $M_V < M_A$, the chiral-symmetry breaking scales Λ_i, and π_T decay constants F_i $(i=L,Q,\psi=1,2,3)$.

Technicolor and QCD are unified at the scale M_V, so that their couplings are equal there, $\alpha_{\rm TC}(M_V)=\alpha_{\rm QCD}(M_V)\equiv\alpha_{\rm ETC}$. Note that this requires that the asymptotic freedom of QCD is lost above the techniquark threshold $2\Lambda_Q$, so that $\alpha_{\rm QCD}$ rises to meet $\alpha_{\rm TC}$ at M_V. We make the approximation that $\alpha_{\rm ETC}$ is constant between M_V and M_A. Once M_V is determined [see Eq. (2.21) below], M_A will be chosen to range from $2M_V$ to $4M_V$. The couplings are evolved down to lower scales $\mu=M_V e^t$ according to the coupled *second-order* β functions [13,14]

$$\begin{aligned}\beta_{\rm TC}(\alpha_{\rm TC},\alpha_{\rm QCD})&\equiv\frac{d\alpha_{\rm TC}}{dt}\\&=-b_{T1}\alpha_{\rm TC}^2-b_{T2}\alpha_{\rm TC}^3+b_{TQ}\alpha_{\rm TC}^2\alpha_{\rm QCD}\ ,\\ \beta_{\rm QCD}(\alpha_{\rm TC},\alpha_{\rm QCD})&\equiv\frac{d\alpha_{\rm QCD}}{dt}\\&=-b_{Q1}\alpha_{\rm QCD}^2-b_{Q2}\alpha_{\rm QCD}^3+b_{\rm QT}\alpha_{\rm QCD}^2\alpha_{\rm TC}\ .\end{aligned}\tag{2.6}$$

The constants in (2.6) are given by [15]

$$\begin{aligned}b_{T1}&=\frac{1}{6\pi}\left[11N_{\rm TC}-8\sum_{T_i}n_{Ti}T_{2i}\theta(M_Ve^t-2\Lambda_i)\right],\\ b_{T2}&=\frac{1}{12\pi^2}\left[17N_{\rm TC}^2-\sum_{T_i}(20N_{\rm TC}+12C_{2i})\right.\\&\qquad\left.\times n_{Ti}T_{2i}\theta(M_Ve^t-2\Lambda_i)\right],\\ b_{TQ}&=\frac{2}{3\pi^2}\theta(M_Ve^t-2\Lambda_Q)\ ,\end{aligned}\tag{2.7}$$

and

$$\begin{aligned}b_{Q1}&=\frac{1}{6\pi}\left[33-8\sum_{i=q,Q}n_{Qi}T_{2i}\theta(M_Ve^t-2\Lambda_i)\right],\\ b_{Q2}&=\frac{1}{12\pi^2}\left[153-76\sum_{i=q,Q}n_{Qi}T_{2i}\theta(M_Ve^t-2\Lambda_i)\right],\\ b_{QT}&=\frac{1}{2\pi^2}C_{2Q}\theta(M_Ve^t-2\Lambda_Q)\ ,\end{aligned}\tag{2.8}$$

where $n_{TL}=N_L, n_{TQ}=3, n_{T\psi}=1, n_{QQ}=N_{\rm TC}$, and $n_{Qq}=N_L+1$ are the number of fermion doublets contributing to a particular term ($\Lambda_q\simeq 0$). The group-theoretic factors are

$$\begin{aligned}&T_{2L}=T_{2Q}=T_{2q}=\tfrac{1}{2},\quad T_{2\psi}=\frac{N_{\rm TC}-2}{2}\ ,\\ &C_{2L}=C_{2Q}=\frac{N_{\rm TC}^2-1}{2N_{\rm TC}},\quad C_{2\psi}=\frac{(N_{\rm TC}-2)(N_{\rm TC}+1)}{N_{\rm TC}}\ .\end{aligned}\tag{2.9}$$

We used $C_2=\frac{4}{3}$ for the SU(3) quadratic Casimirs of q and Q in (2.8).

The slow running of $\alpha_{\rm TC}$ between $2\Lambda_\psi$ and M_V is achieved by the following stratagem: We define the chiral-symmetry-breaking scales Λ_i by the "nonperturbative" formula

$$\gamma_{m_i}(2\Lambda_i)\equiv\gamma_{m_i}(\alpha_{\rm TC}(2\Lambda_i),\alpha_{\rm QCD}(2\Lambda_i))=1\ ,\tag{2.10}$$

where γ_{m_i} is the anomalous dimension of $\bar T_i T_i$ [16,17]. We shall refer to $\alpha_{\rm TC}(2\Lambda_i)$ and $\alpha_{\rm QCD}(2\Lambda_i)$ as "critical couplings" for chiral-symmetry breaking. Now, since the QCD term $b_{TQ}\alpha_{\rm TC}^2\alpha_{\rm QCD}$ in (2.6) is always fairly small, $N_{\rm TC}$ and N_L can be chosen so that, for $2\Lambda_\psi<\mu<M_V$, $\beta_{\rm TC}$ has an infrared fixed point very near to

$$\alpha_{\rm TC}^*=-\frac{b_{T1}}{b_{T2}}\ .\tag{2.11}$$

The optimal choices of $N_{\rm TC}$ and N_L are ones that make $\alpha_{\rm TC}(2\Lambda_\psi)$ only very slightly less than $\alpha_{\rm TC}^*$. [$\alpha_{\rm TC}(2\Lambda_\psi)$ will be given in Eq. (2.18).] Between these two couplings, $\beta_{\rm TC}\simeq -b_{T1}\alpha_{\rm TC}^*(\alpha_{\rm TC}^*-\alpha_{\rm TC})$. Finally, if we choose $\alpha_{\rm ETC}$ slightly less than $\alpha_{\rm TC}(2\Lambda_\psi)$, a large hierarchy between $2\Lambda_\psi$ and M_V is guaranteed [18]. In our calculations, the ETC scale, i.e., the desired value of $M_V/2\Lambda_\psi$ (with $M_V\gtrsim 100$ TeV) is set by adjusting $\alpha_{\rm ETC}$.

To determine the scale Λ_i from the condition $\gamma_{m_i}=1$, we use a "nonperturbative" form for the anomalous dimensions, determined from their second-order perturbation expressions [17]. The perturbative forms are given by [13,14]

$$\begin{aligned}\tfrac{1}{2}\gamma_{m_i}&=c_{iT}\alpha_{\rm TC}+c_{iQ}\alpha_{\rm QCD}\\&\quad+d_{iT}\alpha_{\rm TC}^2+d_{iQ}\alpha_{\rm QCD}^2+d_{i\rm TQ}\alpha_{\rm TC}\alpha_{\rm QCD}\ .\end{aligned}\tag{2.12}$$

The nonvanishing c and d coefficients for $i=1=L$ are

$$\begin{aligned}c_{1T}&=\frac{3}{4\pi}C_{2L}\ ,\\ d_{1T}&=\frac{1}{32\pi^2}C_{2L}\left[3C_{2L}+\frac{97}{3}N_{\rm TC}\right.\\&\qquad\left.-\frac{40}{3}\sum_{T_i}n_{Ti}T_{2i}\theta(M_Ve^t-2\Lambda_i)\right].\end{aligned}\tag{2.13}$$

For $i=2=Q$, they are

$$\begin{aligned}c_{2T}&=\frac{3}{4\pi}C_{2Q}\ ,\\ c_{2Q}&=\frac{1}{\pi}\ ,\\ d_{2T}&=\frac{1}{32\pi^2}C_{2Q}\left[3C_{2Q}+\frac{97}{3}N_{\rm TC}\right.\\&\qquad\left.-\frac{40}{3}\sum_{T_i}n_{Ti}T_{2i}\theta(M_Ve^t-2\Lambda_i)\right],\\ d_{2Q}&=\frac{1}{24\pi^2}\left[101-\frac{40}{3}\sum_{i=q,Q}n_{Qi}T_{2i}\theta(M_Ve^t-2\Lambda_i)\right],\\ d_{2TQ}&=\frac{1}{4\pi^2}C_{2Q}\ .\end{aligned}\tag{2.14}$$

For $i=3=\psi$,

$$c_{3T}=\frac{3}{4\pi}C_{2\psi}\ , \tag{2.15}$$

$$d_{3T}=\frac{1}{32\pi^2}C_{2\psi}\left[C_{2\psi}+\frac{97}{3}N_{\rm TC}-\frac{40}{3}\sum_{T_i}n_{Ti}T_{2i}\theta(M_V e^t-2\Lambda_i)\right]\ .$$

The "nonperturbative" form of the anomalous dimension is [17]

$$\gamma_{m_i}=1-\sqrt{1-4G_{mi}(\alpha_{\rm TC},\alpha_{\rm WCD})}\ , \tag{2.16}$$

where

$$G_{mi}=c_{iT}\alpha_{\rm TC}+c_{iQ}\alpha_{\rm QCD}+(d_{iT}-c_{iT}^2)\alpha_{\rm TC}^2+(d_{iQ}-c_{iQ}^2)\alpha_{\rm QCD}^2+(d_{iTQ}-2c_{iT}c_{iQ})\alpha_{\rm TC}\alpha_{\rm QCD}\ . \tag{2.17}$$

The critical couplings $\alpha_{\rm TC}(2\Lambda_i)$ and $\alpha_{\rm QCD}(2\Lambda_i)$ and, implicitly, the corresponding scales $2\Lambda_i$ are solutions of the equations $G_{mi}(\alpha_{\rm TC}(2\Lambda_i),\alpha_{\rm QCD}(2\Lambda_i))=\frac{1}{4}$. In particular,

$$\alpha_{\rm TC}(2\Lambda_\psi)=\frac{1}{2(\sqrt{d_{3T}}+c_{3T})}\ . \tag{2.18}$$

The conditions $\gamma_{m_i}(2\Lambda_i)=1$ fix only the ratios $M_V/2\Lambda_i$. To introduce a physical energy scale, we use the constraint [19]

$$F_\pi\equiv 2^{-1/4}G_F^{-1/2}=\sqrt{N_L F_L^2+3F_Q^2+F_\psi^2}=246\ {\rm GeV} \tag{2.19}$$

and assume a relation between F_i and Λ_i. Given our ignorance of walking technicolor dynamics, the best we can do is assume that Λ_i/F_i is scaled from the QCD ratio Λ_q/f_π, where $\Lambda_q=\frac{1}{2}M_\rho=385$ MeV and $f_\pi=93$ MeV. Even with this assumption, there remains an uncertainty of how to account for the dimensionalities d_i of the technifermion SU($N_{\rm TC}$) representations [$d_L=d_Q=N_{\rm TC}, d_\psi=\frac{1}{2}N_{\rm TC}(N_{\rm TC}-1)$]. We shall, therefore, consider two scaling rules which then lead to our two classes, A and B, of technihadron masses. The first rule assumes that F_i scales like $\sqrt{d_i}\Lambda_i$; the second rule assumes that F_i/Λ_i is independent of d_i:

$$\text{(A)}\ \ \Lambda_i=F_i\frac{\Lambda_q}{f_\pi}\left[\frac{3}{d_i}\right]^{1/2}\ ,\qquad \text{(B)}\ \ \Lambda_i=F_i\frac{\Lambda_q}{f_\pi}\ . \tag{2.20}$$

Then, with $t_i=-\ln(M_V/2\Lambda_i)$, we have

$$\text{(A)}\ \ M_V=\frac{2\sqrt{3}F_\pi\Lambda_q}{f_\pi\sqrt{\sum_i n_{Ti}d_i e^{2t_i}}}\ ,\qquad \text{(B)}\ \ M_V=\frac{2F_\pi\Lambda_q}{f_\pi\sqrt{\sum_i n_{Ti}e^{2t_i}}}\ . \tag{2.21}$$

Having built this edifice, we must now add the plumbing by relating how we choose $N_{\rm TC}$ and N_L and evolve the walking $\alpha_{\rm TC}$. The TC coupling walks most slowly between $2\Lambda_\psi$ and M_V for $N_{\rm TC}=N_L$ just slightly larger than 6. We choose

$$N_{\rm TC}=N_L=6 \tag{2.22}$$

and multiply b_{T1} by 1.04 for $2\Lambda_\psi<\mu<M_V$ *only*. This makes $\alpha_{\rm TC}^*>\alpha_{\rm TC}(2\Lambda_\psi)$. Below $2\Lambda_\psi$ QCD effects in $\beta_{\rm TC}$ and γ_{m_2} are so small that we invariably find $\Lambda_Q\cong\Lambda_L$. The next "fudge" we make to $\beta_{\rm TC}$ arises from the fact that the decoupling of the ψ technifermions below $2\Lambda_\psi$ makes $\alpha_{\rm TC}$ run so quickly that a large hierarchy does not develop between $\Lambda_L\cong\Lambda_Q$ and Λ_ψ. This is contrary to the expectation in [8] that the chiral-symmetry-breaking scales of different SU($N_{\rm TC}$) representations are widely (perhaps, exponentially) separated. Therefore, to accommodate this expectation and so investigate the phenomenological consequences of such a hierarchy, we *arbitrarily* multiply b_{T1} by $\frac{1}{2}$ in the region $2\Lambda_Q<\mu<2\Lambda_\psi$. We can offer no further justification for this modification of $\beta_{\rm TC}$. On the other hand, there is not much reason to trust any *perturbative* calculation of the β function in a walking gauge theory.

The last rules of the game we need are those for calculating π_T and ρ_T masses. As we have said, we assume the validity of chiral perturbation theory for the ETC interactions to calculate M_{π_T}. These masses involve products of ETC-generated Q and L hard masses m_Q and m_L and $\bar{Q}Q$ and $\bar{L}L$ condensates, and the hard masses themselves involve $\bar{\psi}\psi$ condensates. We shall need a rule for relating these condensates to the corresponding chiral-symmetry-breaking scales Λ_i. The rule for M_{ρ_T} is entirely QCD motivated: the mass of ρ_T is assumed to be given by the sum of its technifermions' constituent masses which, in turn, are the sum of the appropriate Λ_i and hard masses. The reader has been forewarned of the possible pitfalls of these assumptions.

In lowest-order chiral perturbation theory, the π_T masses have the form

$$F_{ij}^2M_{\pi_T}^2(\bar{T}_iT_j)=m_{T_i}(\Lambda)\langle\bar{T}_iT_i\rangle_\Lambda+m_{T_j}(\Lambda)\langle\bar{T}_jT_j\rangle_\Lambda+\text{QCD contributions}\ , \tag{2.23}$$

where F_{ij} is an appropriate combination of π_T decay constants and the hard masses m_{T_i} and condensates $\langle\bar{T}_iT_i\rangle$ are renormalized at the same scale Λ. The condensates *renormalized at the scale* Λ_i are assumed to be given by the QCD-motivated relation [20,21]

$$\text{(A)}\ \langle \bar{T}_i T_i \rangle = 4\pi\kappa_i F_i^3 \left[\frac{3}{d_i}\right]^{1/2}, \qquad \text{(B)}\ \langle \bar{T}_i T_i \rangle = 4\pi\kappa_i F_i^3 . \tag{2.24}$$

For Case A, we have taken account of the fact that F_i scales like $\sqrt{d_i}$ while $\langle \bar{T}_i T_i \rangle$ scales like d_i. The factor κ_i was introduced in [6]. In QCD, $\kappa = 1.7$ is needed in the quark condensate to make the s-quark mass calculated from $m_s = f_\pi^2 M_K^2 / \langle \bar{q}q \rangle = M_K^2 / 4\pi\kappa f_\pi$ agree with the constituent-quark-model formula $m_s = M_{K^*} - M_\rho = M_\phi - M_{K^*}$. To limit the burgeoning number of arbitrary parameters, we shall assume all the κ_i are equal to a single κ which we vary between 1.0 and 2.0 in calculations. Because hard masses are proportional to condensates, π_T masses grow almost linearly with κ. We collect in the Appendix the formulas for the m_{T_i} and M_{π_T} that concern us in this paper.

At any other scale Λ, the condensates and hard masses are given by the usual renormalization-group formulas

$$\langle \bar{T}_i T_i \rangle_\Lambda = \langle \bar{T}_i T_i \rangle \exp\left[\int_{\Lambda_i}^{\Lambda} \frac{d\mu}{\mu} \gamma_{m_i}(\mu)\right], \qquad m_{T_i}(\Lambda) = m_{T_i}(\Lambda_i) \exp\left[-\int_{\Lambda_i}^{\Lambda} \frac{d\mu}{\mu} \gamma_{m_i}(\mu)\right] . \tag{2.25}$$

As discussed in the Introduction, weak isospin breaking in the U and D hard masses mixes the isoscalar and isovector color-octet technirho states ρ_8^{0a} and ρ_8^{1a}. The elements $M_{II'}$ of their 2×2 mass matrix are taken to be

$$M_{00} = 2\Lambda_Q + m_U + m_D + \delta M_{\rm QCD}, \qquad M_{11} = 2\Lambda_Q + m_U + m_D, \qquad M_{01} = M_{10} = m_U - m_D . \tag{2.26}$$

Here, $\delta M_{\rm QCD}$ is the one-QCD-gluon ($\mathcal{G}^a$) annihilation contribution to M_{00}. Following the vector-meson-dominance model for $e^+e^- \to \pi^+\pi^-$, the coupling of ρ_8^{0a} to $\mathcal{G}^a$ is $\sqrt{2} g_{\rm QCD}/g_{\rho_T} = \sqrt{2\alpha_{\rm QCD}/\alpha_{\rho_T}}$, where α_{ρ_T} was given in (2.5) by $\alpha_{\rho_T} \cong 2.97(3/N_{\rm TC})$. The factor of $\sqrt{2}$ arises from the normalization of the $\rho_8^I \to \pi_T\pi_T$ amplitudes in Table I. Then, the annihilation term is

$$\delta M_{\rm QCD} = \frac{\alpha_{\rm QCD}(M_{11})}{\alpha_{\rho_T}} M_{11} . \tag{2.27}$$

This amounts to about a 5% shift in M_{00}. For the ρ_8^{0a} and ρ_8^{1a} to appear as the ideally mixed $\rho_{\bar{D}D}^a$ and $\rho_{\bar{U}U}^a$, it is also necessary that diagonal elements Γ_{00} and Γ_{11} of their width matrix satisfy $|\Gamma_{00}(s) - \Gamma_{11}(s)|/\sqrt{s} \ll 1$. This turns out to be the case in our model calculations.

C. Set-A and -B mass parameters

Dijet and technipion production rates will be calculated in Sec. IV using two sets of input mass parameters, one resulting from the A convention in (2.20) and (2.24), the other from the B convention. Both sets of parameters derive from

$$M_V = 100\ \text{TeV}, \quad M_A = 400\ \text{TeV}, \quad (g_1/g_2)^2 = 1.5, \quad \kappa = 1.5 . \tag{2.28}$$

The Set-A parameters are (all masses are in GeV)

$$\begin{aligned} &F_L = 28, \quad F_Q = 29, \quad F_\psi = 231, \\ &\Lambda_L = 82, \quad \Lambda_Q = 83, \quad \Lambda_\psi = 428, \\ &M_{00} = 342, \quad M_{11} = 326, \quad M_{01} = 114, \\ &M_W = 80, \quad M_{P_1^+} = 172, \quad M_{P_2^+} = 251, \\ &M_{\pi_{\bar{D}U}} = 261, \quad M_{\pi_{\bar{U}U}} = 333, \quad M_{\pi_{\bar{D}D}} = 157, \\ &M_{\pi_{\bar{N}U}} = 280, \quad M_{\pi_{\bar{E}U}} = 218, \\ &M_{\pi_{\bar{N}D}} = 215, \quad M_{\pi_{\bar{E}D}} = 129, \\ &\gamma_W = 0.202, \quad \gamma_1 = -0.109, \quad \gamma_2 = 0.973 ; \end{aligned} \tag{2.29}$$

γ_W, γ_1, and γ_2 are mixing factors that give the $\bar{D}U$ content of W^+, P_1^+, and P_2^+ and which appear in the ρ_8^{1a} decay amplitudes (see Table I).

The Set-B parameters are

$$\begin{aligned} &F_L = 41, \quad F_Q = 43, \quad F_\psi = 212, \\ &\Lambda_L = 172, \quad \Lambda_Q = 177, \quad \Lambda_\psi = 876, \\ &M_{00} = 484, \quad M_{11} = 460, \quad M_{01} = 78, \\ &M_W = 80, \quad M_{P_1^+} = 218, \quad M_{P_2^+} = 311, \\ &M_{\pi_{\bar{D}U}} = 318, \quad M_{\pi_{\bar{U}U}} = 405, \quad M_{\pi_{\bar{D}D}} = 197, \\ &M_{\pi_{\bar{N}U}} = 340, \quad M_{\pi_{\bar{E}U}} = 265, \\ &M_{\pi_{\bar{N}D}} = 263, \quad M_{\pi_{\bar{E}D}} = 158, \\ &\gamma_W = 0.301, \quad \gamma_1 = 0.263, \quad \gamma_2 = 0.917 . \end{aligned} \tag{2.30}$$

We emphasize again that, while these sets of parameters are "typical," they are for illustrative purposes only. We can make the following general remarks about these masses.

(i) As we noted above, all hard masses and π_T masses grow linearly with κ. We shall see in the Appendix that m_U and m_N and, hence, up-down hard-mass splittings grow approximately linearly with $(g_1/g_2)^2$.

(ii) We also anticipated above that $\Lambda_Q \cong \Lambda_L$. This happens because QCD terms in $\beta_{\rm TC}$ and γ_{m_2} are small for energy scales below $2\Lambda_\psi$ and because $\alpha_{\rm TC}$ rises instantly from $\alpha_{\rm TC}(2\Lambda_Q)$ to the slightly larger $\alpha_{\rm TC}(2\Lambda_L)$ once techniquarks decouple from $\beta_{\rm TC}$.

(iii) QCD effects are not always unimportant, however. It is evident from (2.29) and (2.30) that techniquark hard masses are appreciably greater than the corresponding technilepton masses. The reason for this is that QCD terms in γ_{m_2} are exponentiated in scaling from M_V and M_A down to Λ_Q [see (2.25) and Eq. (A5) in the Appendix].

(iv) Many of the qualitative differences between the mass parameters of Sets A and B are easy to understand from (2.20) and (2.21). The scaling of F_i by $\sqrt{3/d_i}$ in Case A requires larger values of $-t_i$ than in Case B to realize the same fixed value of M_V. Hence, $2\Lambda_i = M_V e^{t_i}$ is smaller in Set A than in Set B. The differences in the F_i values are obvious then. The larger Λ_i values in Set B lead to the larger ρ_8^I and π_T masses of this case. This happens despite the fact that technifermion hard masses (renormalized at Λ_i) are somewhat smaller in Set B because the anomalous scaling in (2.25) occurs over a shorter momentum range. This last point also accounts for the somewhat smaller splittings between up and down masses in Case B, as can be seen, for example, in the values for $M_{01} = m_U - m_D$.

(v) We shall find that the ideally mixed ρ_T masses are $M_{\rho_{\bar{D}D}} \simeq M_{00} - M_{01}$ and $M_{\rho_{\bar{U}U}} \simeq M_{00} + M_{01}$. Then, the tendency for the two π_T decay channels of the $\rho_{\bar{D}D}$ and $\rho_{\bar{U}U}$ to be closed is apparent in both sets and especially pronounced in Set A.

(vi) For the range of adjustable parameters $(M_V, M_A, (g_1/g_2)^2$ and $\kappa)$ we considered in our model, we found $M_{\rho_{\bar{D}D}} = 200$–$250$ GeV and $M_{\rho_{\bar{U}U}} = 350$–$550$ GeV in Case A, and $M_{\rho_{\bar{D}D}} = 375$–$425$ GeV and $M_{\rho_{\bar{U}U}} = 500$–$700$ GeV in Case B. In Case A, $M_{\rho_{\bar{D}D}}$ is almost always below the $\pi_T\pi_T$ threshold, while it is always above this threshold in Case B. This leads to rather different phenomenologies in the two cases, but we believe that both can be reasonably well tested at the Tevatron, and we are certain they can at higher-energy hadron colliders.

III. COLOR-OCTET TECHNIRHO PRODUCTION

The ρ_8^I will appear as resonances in hadroproduction of dijets and π_T pairs via the coupling $\sqrt{2} g_{\rm QCD}/g_{\rho_T}$ of $\mathcal{G}^a$ to ρ_8^{0a} and the mixing between ρ_8^{0a} and ρ_8^{1a}. The propagator matrix $D(s)$ for $\mathcal{G}^a$-ρ_8^{0a}-ρ_8^{1a} at squared momentum s is the inverse of the symmetric matrix $D^{-1}(s)$ with elements

$$
\begin{aligned}
&D^{-1}_{\mathcal{G}\mathcal{G}}(s) = s \ , \\
&D^{-1}_{00}(s) = s - M_{00}^2 - M_{01}^2 + i\sqrt{s}\,\Gamma_{00}(s) \ , \\
&D^{-1}_{11}(s) = s - M_{11}^2 - M_{01}^2 + i\sqrt{s}\,\Gamma_{11}(s) \ , \\
&D^{-1}_{\mathcal{G}0}(s) = D^{-1}_{0\mathcal{G}}(s) = -\sqrt{2}\frac{g_{\rm QCD}(s)}{g_{\rho_T}} s \ , \\
&D^{-1}_{\mathcal{G}1}(s) = D^{-1}_{1\mathcal{G}}(s) = 0 \ , \\
&D^{-1}_{01}(s) = D^{-1}_{10}(s) = -(M_{00} + M_{11}) M_{01} + i\sqrt{s}\,\Gamma_{01}(s) \ .
\end{aligned}
\tag{3.1}
$$

The $\pi_T\pi_T$ contributions to the elements of the width matrix $\Gamma(s)$ can be determined from Table I [12]. Dijets contribute only to Γ_{00} and are given by (for five light-quark flavors)

$$
\begin{aligned}
&\Gamma(\rho_8^{0a} \to \bar{q}q) = \frac{5}{3}\frac{\alpha_{\rm QCD}^2(s)}{\alpha_{\rho_T}}\sqrt{s} \ , \\
&\Gamma(\rho_8^{0a} \to \mathcal{G}\mathcal{G}) = \frac{\alpha_{\rm QCD}^2(s)}{\alpha_{\rho_T}}\sqrt{s} \ .
\end{aligned}
\tag{3.2}
$$

By construction, $D(s)$ has a gluon pole at $s=0$, consistent with SU(3) gauge invariance. It has ρ_T poles at the zeros of

$$
\begin{aligned}
\frac{1}{s}\det D^{-1}(s) = &\left[s\left[1 - 2\frac{\alpha_{\rm QCD}(s)}{\alpha_{\rho_T}}\right] - M_{00}^2 - M_{01}^2 + i\sqrt{s}\,\Gamma_{00}(s) \right] [s - M_{11}^2 - M_{01}^2 + i\sqrt{s}\,\Gamma_{11}(s)] \\
&- [(M_{00} + M_{11}) M_{01} - i\sqrt{s}\,\Gamma_{01}(s)]^2 \ .
\end{aligned}
\tag{3.3}
$$

A. Dijet production

We present here the dijet invariant-mass distribution $d\sigma(p^{\pm}p \to \text{jet jet})/d\mathcal{M}$ (see, e.g. [1]) modified to include ρ_8^I resonances. This distribution is obtained from the cross sections for the $2 \to 2$ subprocesses in $O(\alpha_{\rm QCD}^2)$ by replacing $1/p^2$ in the gluon propagator by $D_{\mathcal{G}\mathcal{G}}(p^2)$. It is an excellent approximation (and simplifies computation) to make this replacement only for s-channel gluon propagators [22]. Then, the modified subprocesses are $\bar{q}_i q_i \to \bar{q}_j q_j$ $(j \neq i)$, $\bar{q}_i q_i \to \bar{q}_i q_i$, $\bar{q}_i q_i \to \mathcal{G}\mathcal{G}$, $\mathcal{G}\mathcal{G} \to \bar{q}_i q_i$, and $\mathcal{G}\mathcal{G} \to \mathcal{G}\mathcal{G}$. Here, $i,j = 1, \ldots, n_F$, where n_F is the number of light-quark flavors. We take $n_F = 5$ for the S$\bar{p}p$S and Tevatron colliders and $n_F = 6$ for the LHC and SSC.

We express the subprocesses cross sections in terms of the squared center-of-mass energy $\hat{s} \equiv \mathcal{M}^2$, the scattering angle $z \equiv \cos\theta = 2\hat{t}/\hat{s} + 1$ (with $\hat{s} + \hat{t} + \hat{u} = 0$), and the $\mathcal{G}\mathcal{G}$ element of the dimensionless propagator matrix

$$
\mathcal{D}(\hat{s}) = \hat{s} D(\hat{s}) \ . \tag{3.4}
$$

The cross sections are give by (with $j \neq i = 1, \ldots, n_F$)

$$
\frac{d\hat{\sigma}\left[\bar{q}_i q_i \to \sum_{j \neq i} \bar{q}_j q_j\right]}{dz} = \frac{\pi\alpha_{\rm QCD}^2 (n_F - 1)}{9\hat{s}} |\mathcal{D}_{\mathcal{G}\mathcal{G}}(\hat{s})|^2 (1 + z^2) \ , \tag{3.5}
$$

$$
\frac{d\hat{\sigma}(\bar{q}_i q_i \to \bar{q}_i q_i)}{dz} = \frac{\pi\alpha_{\rm QCD}^2}{9\hat{s}} \left[|\mathcal{D}_{\mathcal{G}\mathcal{G}}(\hat{s})|^2 (1 + z^2) + \tfrac{2}{3} \mathrm{Re}\mathcal{D}_{\mathcal{G}\mathcal{G}}(\hat{s}) \frac{(1+z)^2}{1-z} + \frac{2[4 + (1+z)^2]}{(1-z)^2} \right] , \tag{3.6}
$$

$$\frac{d\hat{\sigma}(\bar{q}_i q_i \to \mathcal{G}\mathcal{G})}{dz} = \frac{64}{9n_F}\frac{d\hat{\sigma}(\mathcal{G}\mathcal{G}\to\bar{q}_i q_i)}{dz} = \frac{2\pi\alpha_{\rm QCD}^2}{3\hat{s}}\left[|\mathcal{D}_{\mathcal{G}\mathcal{G}}(\hat{s})-1|^2(1-z^2)+\frac{16}{9}\left[\frac{1+z^2}{1-z^2}\right]-(1+z^2)\right], \tag{3.7}$$

$$\frac{d\hat{\sigma}(\mathcal{G}\mathcal{G}\to\mathcal{G}\mathcal{G})}{dz} = \frac{9\pi\alpha_{\rm QCD}^2}{4\hat{s}}\left[\tfrac{1}{4}|\mathcal{D}_{\mathcal{G}\mathcal{G}}(\hat{s})-1|^2 z^2 - {\rm Re}[\mathcal{D}_{\mathcal{G}\mathcal{G}}(\hat{s})-1]\frac{z^2}{1-z^2}+3-\tfrac{1}{4}(1-z^2)+\frac{2(1+z)}{(1-z)^2}+\frac{2(1-z)}{(1+z)^2}\right], \tag{3.8}$$

$$\frac{d\hat{\sigma}(q_i q_j \to q_i q_j)}{dz} = \frac{d\hat{\sigma}(\bar{q}_i\bar{q}_j\to\bar{q}_i\bar{q}_j)}{dz} = \frac{d\hat{\sigma}(q_i\bar{q}_j\to q_i\bar{q}_j)}{dz} = \frac{2\pi\alpha_{\rm QCD}^2}{9\hat{s}}\left[\frac{4+(1+z)^2}{(1-z)^2}\right], \tag{3.9}$$

$$\frac{d\hat{\sigma}(q_i q_i \to q_i q_i)}{dz} = \frac{d\hat{\sigma}(\bar{q}_i\bar{q}_i\to\bar{q}_i\bar{q}_i)}{dz} = \frac{2\pi\alpha_{\rm QCD}^2}{9\hat{s}}\left[\frac{4+(1+z)^2}{(1-z)^2}+\frac{4+(1-z)^2}{(1+z)^2}-\frac{8}{3(1-z^2)}\right], \tag{3.10}$$

$$\frac{d\hat{\sigma}(\mathcal{G}q_i \to \mathcal{G}q_i)}{dz} = \frac{d\hat{\sigma}(\mathcal{G}\bar{q}_i\to\mathcal{G}\bar{q}_i)}{dz} = \frac{\pi\alpha_{\rm QCD}^2}{2\hat{s}}[4+(1+z)^2]\left[\frac{1}{(1-z)^2}+\frac{2}{9(1+z)}\right]. \tag{3.11}$$

In our calculations of dijet (and $\pi_T\pi_T$) production below, the running QCD coupling $\alpha_{\rm QCD}$ in these cross sections will be evaluated at $Q^2=\hat{s}$ from the "standard" formula $\alpha_{\rm QCD}(\hat{s})\cong 12\pi/[(33-2n_F)\ln(\hat{s}/\Lambda_{\rm QCD}^2)]$, with $\Lambda_{\rm QCD}=200$ MeV. We use this formula, which gives a value of $\alpha_{\rm QCD}(\hat{s})$ approximately 50% larger than the coupling evolved from (2.6), in order to compare more directly with experiment. The important point is that we choose the Q^2 of the process to be $\hat{s}$, rather than p_T^2 or $p_T^2/4$, because we are concerned with the production of states having invariant mass $\mathcal{M}=\sqrt{\hat{s}}$. The different choices of Q^2 can make at least a 25–50 % difference in the overall scale of $d\sigma(p^{\pm}p\to\text{jet jet})/d\mathcal{M}$. This should be taken into account in comparing our theoretical cross sections with dijet data.

We shall see in Sec. IV that the largest signal for ρ_8^I production occurs in dijets with $\bar{q}q$ final states. This signal comes mainly from $\bar{q}_i q_i\to\bar{q}_j q_j$ $(j\neq i)$. The ρ_8^I signal in other subprocesses tends to be overwhelmed by the $\hat{t}$- and $\hat{u}$-channel poles (at $z=\pm1$) in the cross sections. In all cases, the signal-to-background ratio is enhanced by making a hard cut on jet rapidities.

The dijet invariant-mass distribution in a $p^{\pm}p$ collider with center-of-mass energy $\sqrt{s}$, where both jets are required to have rapidity $|y_{1,2}|<Y$, is given by

$$\frac{d\sigma(p^{\pm}p\to\text{jet jet})}{d\mathcal{M}} = \frac{2\mathcal{M}}{s}\int_{-Y_B}^{Y_B}dy_B\int_{-z_0}^{z_0}dz\sum_{i,j}f_i^{(p^{\pm})}(\sqrt{\tau}e^{y_B})f_j^{(p)}(\sqrt{\tau}e^{-y_B})\frac{1}{2}\sum_{k,l}\frac{d\hat{\sigma}(ij\to kl)}{dz}. \tag{3.12}$$

In (3.12), $\tau=\mathcal{M}^2/s$, y_B is the boost rapidity of the subprocess frame, and the rapidities y_1, y_2 of the produced jets are related to y_B and z by $y_{1,2}=y_B\pm\frac{1}{2}\ln[(1+z)/(1-z)]$. The cut on jet rapidities corresponds to the limits

$$Y_B=\min(Y,-\tfrac{1}{2}\ln\tau),\qquad z_0=\min(1,\tanh(Y-|y_B|)). \tag{3.13}$$

The factor of $\frac{1}{2}$ multiplying the subprocess cross sections prevents double counting both distinct $(k\neq l)$ and identical-particle final states. We shall use the Eichten-Hinchliffe-Lane-Quigg (EHLQ) Set-1 of parton distribution function $f_i^{(p^{\pm})}(x,Q^2)$, with $Q^2=\mathcal{M}^2$ and $\Lambda_{\rm QCD}=200$ MeV, to calculate the dijet mass distributions in (3.12). The distributions at various hadron colliders that result from our Sets A and B of technihadron masses will be presented in Sec. IV.

B. Technipion pair production

Technipions are pair produced in hadron collisions through two subprocesses that are ρ_8^I dominated [1]. The first is quark-antiquark annihilation to a single gluon. Color-octet $(\pi_{\bar{Q}Q}\pi_{\bar{Q}Q})$ and -triplet $(\pi_{\bar{Q}L}\pi_{\bar{L}Q})$ pairs may then be produced via their coupling to $\mathcal{G}^a$ and to ρ_8^{0a} and ρ_8^{1a}. $W^+\pi_{\bar{U}D}$ and $P_i^+\pi_{\bar{U}D}$ are produced from ρ_8^{1a} only. The cross section for this process, averaged over $\bar{q}q$ colors and summed over the colors B,C of a specific pair of technipions, is given by

$$\sum_{B,C}\frac{d\hat{\sigma}(\bar{q}_i q_i\to\pi_B\pi_C)}{dz} = \frac{\pi\alpha_{\rm QCD}^2(\hat{s})\beta^3}{72\hat{s}}\mathcal{S}_{BC}(1-z^2)\times\sum_{a=1}^{8}\sum_{B,C}|\mathcal{D}_{\mathcal{G}\mathcal{G}}^{aBC}+\mathcal{D}_{\mathcal{G}0}^{aBC}+\mathcal{D}_{\mathcal{G}1}^{aBC}|^2. \tag{3.14}$$

The counting factor $\mathcal{S}_{BC}=N_L$ for each channel of $\pi_{\bar{L}Q}\pi_{\bar{Q}L}$ production because technilepton flavor symmetry is left unbroken in our calculations; $\mathcal{S}_{BC}=1$ for $\pi_{\bar{D}U}\pi_{\bar{U}D}$ and $\mathcal{S}_{BC}=\frac{1}{2}$ for the identical-particle final states $\pi_{\bar{U}U}\pi_{\bar{U}U}$ and $\pi_{\bar{D}D}\pi_{\bar{D}D}$. $\beta=2k/\sqrt{\hat{s}}$ is the velocity of π_B in the subprocesses frame *when* $M_{\pi_B}=M_{\pi_C}$, where k is the magnitude of the π_T momentum in this frame. The propagator factors are given by

$$\mathcal{D}_{\mathcal{G}\mathcal{G}}^{aBC}=\mathcal{D}_{\mathcal{G}\mathcal{G}}(\hat{s})C_0^{aBC},\qquad \mathcal{D}_{\mathcal{G}0}^{aBC}=\frac{g_{\rho_T}}{\sqrt{2}g_{\rm QCD}}\mathcal{D}_{\mathcal{G}0}(\hat{s})C_0^{aBC},\qquad \mathcal{D}_{\mathcal{G}1}^{aBC}=\frac{g_{\rho_T}}{\sqrt{2}g_{\rm QCD}}\mathcal{D}_{\mathcal{G}1}(\hat{s})C_1^{aBC}, \tag{3.15}$$

where C_0^{aBC} and C_1^{aBC} were given in Table I.

The second subprocess is technipion pair production from two QCD gluons. There are four graphs for this process in $O(\alpha_{\rm QCD})$ dictated by gauge invariance: two-gluon annihilation to a single gluon, as in the $\bar{q}q$ processes; $\hat{t}$- and $\hat{u}$-channel exchange of technipions; and a $\mathcal{G}\mathcal{G}\pi_T\pi_T$ direct coupling [1]. The last three graphs occur only for color-octet and color-triplet pair production. The cross section, averaged over initial gluon colors, is given by

$$\sum_{B,C}\frac{d\hat{\sigma}(\mathcal{G}\mathcal{G}\to\pi_B\pi_C)}{dz}=\frac{\pi\alpha_{\rm QCD}^2(\hat{s})\beta}{\hat{s}}\mathcal{S}_{BC}$$
$$\times\left\{\frac{3}{32}\beta^2z^2\left[\frac{1}{8}\sum_{a=1}^{8}\sum_{B,C}|\mathcal{D}_{\mathcal{G}\mathcal{G}}^{aBC}+\mathcal{D}_{\mathcal{G}0}^{aBC}+\mathcal{D}_{\mathcal{G}1}^{aBC}|^2-\frac{2\beta^2(1-z^2)}{1-\beta^2z^2}T(R)\mathrm{Re}(\mathcal{D}_{\mathcal{G}\mathcal{G}}+\mathcal{D}_{\mathcal{G}0}+\eta_{BC}\mathcal{D}_{\mathcal{G}1})\right.\right.$$
$$\left.\left.+2T(R)\left[\frac{\beta^2(1-z^2)}{1-\beta^2z^2}\right]^2\right]+T(R)\left[\frac{T(R)}{d(R)}-\frac{3}{32}\right]\left[\frac{(1-\beta^2)^2+\beta^4(1-z^2)^2}{(1-\beta^2z^2)^2}\right]\right\}. \tag{3.16}$$

Here, R is the SU(3) representation of the π_T. $T(R)$ is the trace of the square of their SU(3)-generator matrices; $T(R)=\frac{1}{2}$ for triplets [$d(R)=3$], 3 for octets [$d(R)=8$]. Note that only the first term in (3.16) contributes to $W^+\pi_{\bar{U}D}$ and $P_i^+\pi_{\bar{U}D}$ production. The factor $\eta_{BC}=1$ for $\pi_{\bar{U}U}\pi_{\bar{U}U}$, $\pi_{\bar{U}N}\pi_{\bar{N}U}$, and $\pi_{\bar{U}E}\pi_{\bar{E}U}$; $\eta_{BC}=-1$ for $\pi_{\bar{D}D}\pi_{\bar{D}D}$, $\pi_{\bar{D}N}\pi_{\bar{N}D}$, and $\pi_{\bar{D}E}\pi_{\bar{E}D}$; $\eta_{BC}=0$ for $\pi_{\bar{D}U}\pi_{\bar{U}D}$ since there is no interference between the $\hat{t}$- and $\hat{u}$-exchange terms and the ρ_8^{1a} term in this case.

The $\pi_T\pi_T$ invariant-mass distribution in $p^{\pm}p$ collisions, where both technipions are required to have rapidity $|y_{1,2}|<Y$, is given by

$$\sum_{B,C}\frac{d\sigma(p^{\pm}p\to\pi_B\pi_C)}{d\mathcal{M}}=\frac{2\mathcal{M}}{s}\int_{-Y_B}^{Y_B}dy_B\int_{z_1}^{z_2}dz$$
$$\times\left[\sum_i[f_{q_i}^{(p^{\pm})}(\sqrt{\tau}e^{y_B})f_{\bar{q}_i}^{(p)}(\sqrt{\tau}e^{-y_B})+f_{\bar{q}_i}^{(p^{\pm})}(\sqrt{\tau}e^{y_B})f_{q_i}^{(p)}(\sqrt{\tau}e^{-y_B})]\right.$$
$$\times\sum_{B,C}\frac{d\hat{\sigma}(\bar{q}_iq_i\to\pi_B\pi_C)}{dz}+f_{\mathcal{G}}^{(p^{\pm})}(\sqrt{\tau}e^{y_B})f_{\mathcal{G}}^{(p)}(\sqrt{\tau}e^{y_B})$$
$$\left.\times\sum_{B,C}\frac{d\hat{\sigma}(\mathcal{G}\mathcal{G}\to\pi_B\pi_C)}{dz}\right]. \tag{3.17}$$

As in the dijet invariant-mass distribution, the EHLQ Set-1 parton distribution functions are used with $Q^2=\mathcal{M}^2$. The ranges of the integrals that enforce the cut on π_T rapidities are obtained as follows: let $v_{1,2}=k/E_{1,2}$ be the velocities of π_B and π_C in the subprocess frame. Then, the limits on their rapidities *in this frame* are

$$y_{i\,\min}^*=\max\left[-(Y+y_B),-\ln\left[\frac{1+v_i}{1-v_i}\right]^{1/2}\right],$$
$$y_{i\,\max}^*=\min\left[Y-y_B,\ln\left[\frac{1+v_i}{1-v_i}\right]^{1/2}\right], \tag{3.18}$$

and the limits on the integrals are given by

$$Y_B=\min(Y,-\tfrac{1}{2}\ln\tau),$$
$$z_1=\max\left[-1,\frac{1}{v_1}\tanh y_{1\,\min}^*,-\frac{1}{v_2}\tanh y_{2\,\max}^*\right],$$
$$z_2=\min\left[1,\frac{1}{v_1}\tanh y_{1\,\max}^*,-\frac{1}{v_2}\tanh y_{2\,\min}^*\right]. \tag{3.19}$$

Of course, these reduce to the limits in (3.13) when $M_{\pi_B}=M_{\pi_C}=0$. The production rates for $\pi_T\pi_T$ and our expectations for their detectability will be discussed in Sec. IV.

IV. DIJET AND TECHNIPION PRODUCTION RATES IN HADRON COLLIDERS

In this section we present our results for $\rho_{\bar{Q}Q}$ production at hadron colliders in the dijet and $\pi_T\pi_T$ channels, first for the Set-A input parameters, then for Set B. Much of our discussion is concentrated on signals at the Fermilab Tevatron because it is possible that several of them are now, or soon will be, within reach of experiments there. For dijets, we pay attention to the effect of jet resolution smearing and rapidity cuts. We find that only the $\rho_{\bar{D}D}$ expected in Set A is likely to have a dijet signal strong enough to be excluded soon. Production of $\pi_T\pi_T$ is interesting and fairly copious for both parameter sets, with several important channels having cross sections in the 10-pb range at the Fermilab Tevatron and

1000 times larger at the SSC. These channels are conventionally expected to decay to $\bar{b}\tau^- b\tau^+$, $\bar{b}b\bar{b}b$, and $\bar{t}\tau^- t\tau^+$. Detailed detector-specific studies are needed to study the backgrounds and decide the reach for these modes in various experiments.

Again, we caution the reader that the technihadron masses and production rates emerging from our model calculations are, at best, illustrative of what should be expected from a multiscale model of walking technicolor. Our detailed mass values can vary by 25–100 GeV, with corresponding changes in cross sections. We shall try to give some feeling for this in our discussion of dijet production below.

A. Set A parameters

We record again the technihadron masses (in GeV) and the mixing factors for the $\bar{D}U$ content of W^+, P_1^+, and P_2^+ of Set A that we use to compute dijet and technipion production rates:

$$\begin{aligned}
&M_{00}=342,\quad M_{11}=326,\quad M_{01}=114\ ,\\
&M_W=80,\quad M_{P_1^+}=172,\quad M_{P_2^+}=251\ ,\\
&M_{\pi_{\bar{D}U}}=261,\quad M_{\pi_{\bar{U}U}}=333,\quad M_{\pi_{\bar{D}D}}=157\ ,\\
&M_{\pi_{\bar{N}U}}=280,\quad M_{\pi_{\bar{E}U}}=218\ ,\\
&M_{\pi_{\bar{N}D}}=215,\quad M_{\pi_{\bar{E}D}}=129\ ,\\
&\gamma_W=0.202,\quad \gamma_1=-0.109,\quad \gamma_2=0.973\ .
\end{aligned}\tag{4.1}$$

We find that the ρ_8^I appear as nearly, but not completely, ideally mixed resonances with $M_{\rho_{\bar{D}D}}\cong 228$ GeV and $M_{\rho_{\bar{U}U}}\cong 465$ GeV. Thus, the only allowed decay modes of $\rho_{\bar{D}D}$ are $\bar{q}_i q_i$ $(i=1,\ldots,5)$ and $\mathcal{G}\mathcal{G}$ with the rates

$$\begin{aligned}
\Gamma(\rho_{\bar{D}D}\to\bar{q}q)&=\frac{5}{6}\frac{\alpha_{\rm QCD}^2}{\alpha_{\rho_T}}M_{\rho_{\bar{D}D}}\simeq 1.7\ \text{GeV}\ ,\\
\Gamma(\rho_{\bar{D}D}\to\mathcal{G}\mathcal{G})&=\frac{1}{2}\frac{\alpha_{\rm QCD}^2}{\alpha_{\rho_T}}M_{\rho_{\bar{D}D}}\simeq 1.0\ \text{GeV}\ .
\end{aligned}\tag{4.2}$$

The corresponding rates for $\rho_{\bar{U}U}$ are 2.9 GeV and 1.8 GeV. We shall see that its $\pi_T\pi_T$ width is about 15 GeV. The only such channels open for $\rho_{\bar{U}U}$ are $\pi_{\bar{D}E}\pi_{\bar{E}D}$, $\pi_{\bar{D}N}\pi_{\bar{N}D}$, $\pi_{\bar{U}E}\pi_{\bar{E}U}$, $\pi_{\bar{D}D}\pi_{\bar{D}D}$, $W^+\pi_{\bar{U}D}$, and $P_1^+\pi_{\bar{U}D}$. By far the largest decay modes are $\pi_{\bar{D}E}\pi_{\bar{E}D}$ and $\pi_{\bar{U}E}\pi_{\bar{E}U}$.

In Fig. 1 we show the dijet invariant-mass distribution at the Tevatron $\bar{p}p$ collider with $\sqrt{s}=1800$ GeV. The cut on the jet rapidities is the same as that used by the CDF Collaboration in their ongoing analysis of dijets, $Y=0.7$ [23]. The $\rho_{\bar{D}D}$ appears as a striking narrow resonance of width $\simeq 4$ GeV at 228 GeV, the $\rho_{\bar{U}U}$ as a broader ($\simeq 20$ GeV), much less accessible one at 465 GeV. It is clear that both resonances show most clearly in jets with $\bar{q}q$ final states. As we noted earlier, the resonance in $\mathcal{G}\mathcal{G}$ jets is diluted by the fairly large nonresonant $\hat{t}$ and $\hat{u}$ channel and direct four-gluon contributions. In searching for these resonances it would be a boon if experimentalists could efficiently distinguish between quark jets and gluon jets. The integral over the $\rho_{\bar{D}D}$ resonance region (from 223 to 233 GeV) is

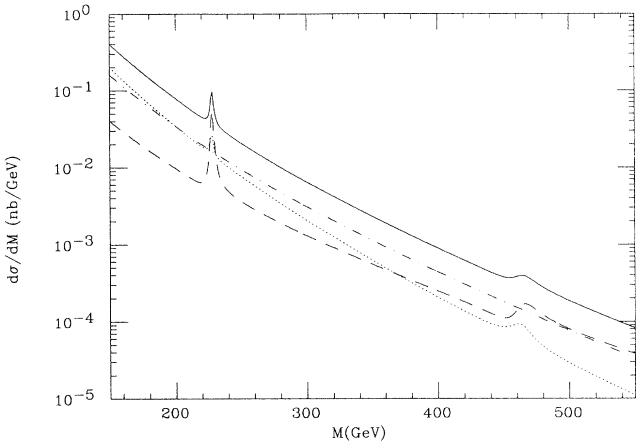

FIG. 1. The dijet invariant-mass distribution for $\bar{p}p$ collisions at $\sqrt{s}=1800$ GeV (solid curve). Set-A input masses were used and cross sections calculated using the EHLQ Set-1 distribution functions with $Q^2=\mathcal{M}^2$. Both jets have rapidity $|y|<0.7$. The qq (dashed), $\mathcal{G}\mathcal{G}$ (dotted), and $q\mathcal{G}$ (dashed-dotted) components are shown separately.

$$\sigma_{\rho_{\bar{D}D}}(Y=0.70)=565\ \text{pb},\quad \sigma_{\rm bkgd}(Y=0.70)=360\ \text{pb}\ .\tag{4.3}$$

The integral over the $\rho_{\bar{U}U}$ region (from 455 to 475 GeV) is

$$\sigma_{\rho_{\bar{U}U}}(Y=0.70)=7.4\ \text{pb},\quad \sigma_{\rm bkgd}(Y=0.70)=6.0\ \text{pb}\ .\tag{4.4}$$

That is, the *theoretical* signal-to-background (S/B) ratio is about $\frac{1}{2}$ for $\rho_{\bar{D}D}$ and $\frac{1}{4}$ for $\rho_{\bar{U}U}$. The CDF Collaboration has collected approximately 4.7 pb^{-1} of dijet data (up to $\mathcal{M}=1000$ GeV) which is still undergoing analysis. The Tevatron collider is expected to provide an additional 50–100 pb^{-1} of data to CDF and D0 in its next run. Theoretically, then, this $\rho_{\bar{D}D}$ can be excluded with existing data and the $\rho_{\bar{U}U}$ with data from the next run.

Unfortunately, these theoretical expectations for signal-to-background ratio are significantly worsened by the finite resolution of the detectors. For CDF, the dijet invariant-mass resolution is $\Delta\mathcal{M}/\mathcal{M}\simeq 0.1$ [24]. The effects of including this resolution (with Gaussian smearing) are illustrated in Fig. 2. Let us concentrate on the $\rho_{\bar{D}D}$ region which we show in close-up, with its background, in Fig. 3. The total and nonresonant cross sections in a bin of width $\delta\mathcal{M}$ centered on the resonance are

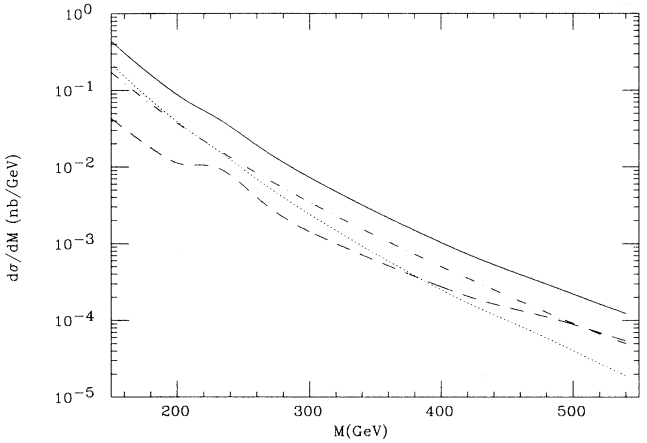

FIG. 2. The dijet invariant-mass distributions for $\bar{p}p$ collisions at $\sqrt{s}=1800$ GeV assuming a resolution of $\Delta\mathcal{M}/\mathcal{M}=0.1$. Set A input masses were used. Both jets have rapidity $|y|<0.7$. The curves are labeled as in Fig. 1.

$$\sigma_{\rho_{\bar{D}D}}(Y=0.70)=455\text{ pb},\quad \sigma_{\text{bkgd}}(Y=0.70)=400\text{ pb}\quad(\delta\mathcal{M}=10\text{ GeV}),$$
$$\sigma_{\rho_{\bar{D}D}}(Y=0.70)=1.00\text{ nb},\quad \sigma_{\text{bkgd}}(Y=0.70)=0.89\text{ nb}\quad(\delta\mathcal{M}=23\text{ GeV}),\qquad(4.5)$$
$$\sigma_{\rho_{\bar{D}D}}(Y=0.70)=2.16\text{ nb},\quad \sigma_{\text{bkgd}}(Y=0.70)=1.97\text{ nb}\quad(\delta\mathcal{M}=46\text{ GeV}).$$

While these signals represent 5–10 standard deviation effects in the existing data, the CDF resolution degrades S/B to about $\frac{1}{10}$. With 10% resolution, a search for $\rho_{\bar{D}D}$ would not be a simple matter of bump hunting. One strategy (followed, e.g., by the UA2 Collaboration in its search for the W and Z bosons in dijets [25]) is the following. Assume a mass [and width from Eq. (4.2)] for the $\rho_{\bar{D}D}$. Then fit the data for $|\mathcal{M}-M_{\rho_{\bar{D}D}}|\gtrsim 0.1M_{\rho_{\bar{D}D}}$ to the shape expected from QCD and look for an excess in the $\rho_{\bar{D}D}$ region that fits a resolution-smeared resonance. Determining the significance of a smeared resonance is a job best left to the experimentalists. Therefore, from now on we shall quote only the theoretical (unsmeared) signal and background rates.

The effects of changing the rapidity cut Y are shown in Figs. 4–6, in which we present the dijet cross section for $Y=0.35$, 1.5, and 2.5. The total and background cross sections in the 10-GeV wide $\rho_{\bar{D}D}$ region are

$$\sigma_{\rho_{\bar{D}D}}(Y=0.35)=140\text{ pb},\quad \sigma_{\text{bkgd}}(Y=0.35)=80\text{ pb},$$
$$\sigma_{\rho_{\bar{D}D}}(Y=1.5)=3.4\text{ nb},\quad \sigma_{\text{bkgd}}(Y=1.5)=2.8\text{ nb},\qquad(4.6)$$
$$\sigma_{\rho_{\bar{D}D}}(Y=2.5)=23.5\text{ nb},\quad \sigma_{\text{bkgd}}(Y=2.5)=22.7\text{ nb}.$$

The signal-to-background ratio worsens as the rapidity cut is loosened because of the increase in $\mathcal{GG}$ jets. The narrow rapidity range used by CDF in its analysis is thus well suited to the search for narrow $\bar{q}q$ resonances in dijet production.

As a measure of the sensitivity of these dijet cross sections to the input mass parameters, we have computed them for three other sets of input mass parameters.

(i) In the first set, $M_{\rho_{\bar{D}D}}=200$ GeV and $M_{\rho_{\bar{U}U}}=465$ GeV. The total and background cross sections in the 10-GeV bin containing the $\rho_{\bar{D}D}$ are $\sigma_{\rho_{\bar{D}D}}=1.11$ nb and $\sigma_{\text{bkgd}}=0.75$ nb. For the 20-GeV bin containing the $\rho_{\bar{U}U}$ they are $\sigma_{\rho_{\bar{U}U}}=12$ pb and $\sigma_{\text{bkgd}}=6$ pb.

(ii) In the second set, $M_{\rho_{\bar{D}D}}=245$ GeV and $M_{\rho_{\bar{U}U}}=560$ GeV. The cross sections in the 10-GeV-wide $\rho_{\bar{D}D}$ bin are

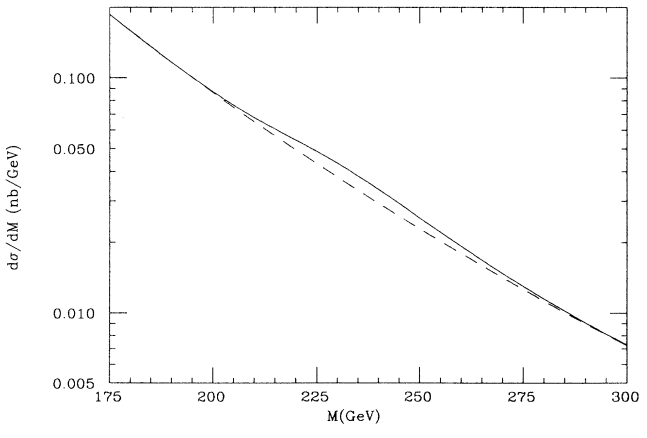

FIG. 3. The $\rho_{\bar{D}D}$ dijet signal (solid curve) and background (dashed curve) for $\bar{p}p$ collisions at $\sqrt{s}=1800$ GeV assuming a resolution of $\Delta\mathcal{M}/\mathcal{M}=0.1$. Set A input masses were used. Both jets have rapidity $|y|<0.7$.

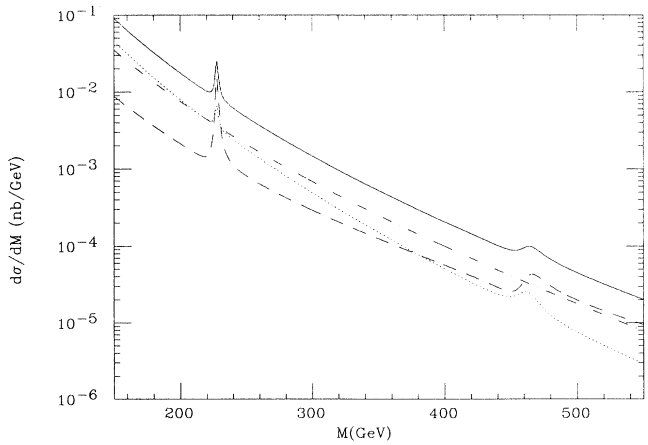

FIG. 4. The unsmeared dijet invariant-mass distribution for $\bar{p}p$ collisions at $\sqrt{s}=1800$ GeV. Set-A input masses were used. Both jets have rapidity $|y|<0.35$. The curves are labeled as in Fig. 1.

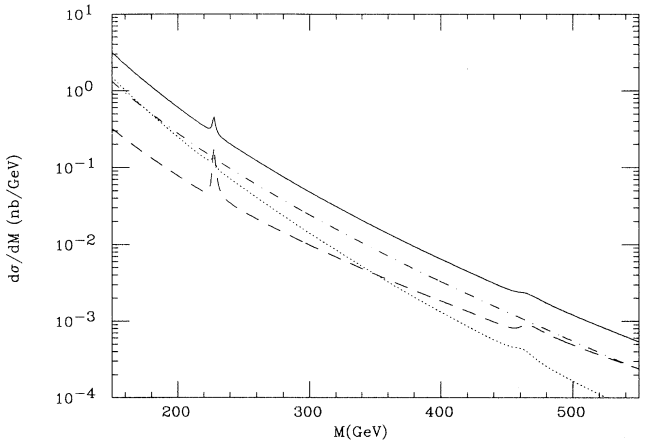

FIG. 5. The unsmeared dijet invariant-mass distribution for $\bar{p}p$ collisions at $\sqrt{s}=1800$ GeV. Both jets have rapidity $|y|<1.5$. The curves are labeled as in Fig. 1.

$\sigma_{\rho_{\bar{D}D}}=385$ pb and $\sigma_{\text{bkgd}}=235$ pb; in the 20-GeV-wide $\rho_{\bar{U}U}$ bin they are $\sigma_{\rho_{\bar{U}U}}=3.5$ pb and $\sigma_{\text{bkgd}}=1.3$ pb. In both these cases, S/B for the $\rho_{\bar{U}U}$ is significantly better than in Eq. (4.4), so it is barely possible that experiments at the upgraded Tevatron (with an integrated luminosity of 100 pb or so) will be able to test for the presence of the $\rho_{\bar{U}U}$.

(iii) Finally, lest the weak isospin breaking in our "typical" Set A masses be considered uncomfortably large, we have examined a case with smaller M_{01}. This set corresponds to $M_V=200$ TeV, $M_A=800$ TeV, $(g_1/g_2)^2=1.0$, and $\kappa=2.0$. The scales Λ_i are the same as in (2.29) and the technihadron masses (in GeV) and mixing factors are

$$
\begin{aligned}
&M_{00}=281,\quad M_{11}=269,\quad M_{01}=65\ ,\\
&M_W=80,\quad M_{P_1^+}=160,\quad M_{P_2^+}=234\ ,\\
&M_{\pi_{\bar{D}U}}=239,\quad M_{\pi_{\bar{U}U}}=299,\quad M_{\pi_{\bar{D}D}}=157\ ,\\
&M_{\pi_{\bar{N}U}}=251,\quad M_{\pi_{\bar{E}U}}=201\ ,\\
&M_{\pi_{\bar{N}D}}=199,\quad M_{\pi_{\bar{E}D}}=131\ ,\\
&\gamma_W=0.198,\quad \gamma_1=-0.105,\quad \gamma_2=0.975\ .
\end{aligned}
\tag{4.7}
$$

The theoretical and smeared dijet cross sections at the Tevatron are shown in Figs. 7 and 8. The resonances appear at $M_{\rho_{\bar{D}D}}=220$ GeV and $M_{\rho_{\bar{U}U}}=355$ GeV with widths of $\Gamma_{\rho_{\bar{D}D}}\simeq 4$ GeV and $\Gamma_{\rho_{\bar{U}U}}\simeq 15$ GeV. The theoretical cross section in the 10-GeV bin surrounding $\rho_{\bar{D}D}$ is $\sigma_{\rho_{\bar{D}D}}=720$ pb with a background of 485 pb. In the 20-GeV bin containing $\rho_{\bar{U}U}$, the cross section is $\sigma_{\rho_{\bar{U}U}}=70$ pb with a background of 40 pb. In this case both $\rho_{\bar{Q}Q}$ signals may be accessible and excluded with the existing data.

Let us return to the Set-A mass inputs and consider their dijet signals in other hadron colliders. The theoretical and smeared $\rho_{\bar{Q}Q}$ signals are shown in Figs. 9 and 10 for the S$\bar{p}p$S collider. Again, we used a rapidity cut of $Y=0.7$ and a 10% dijet mass resolution, which is correct for the data taken by the UA2 Collaboration [25]. The UA2 data is also based on an integrated luminosity of 4.7 pb^{-1}. The theoretical dijet rates are shown in Fig. 11 for the LHC (assuming $\sqrt{s}=17$ TeV) and in Fig. 12 for the SSC. The theoretical cross sections in a 10-GeV bin about the $\rho_{\bar{D}D}$ and a 20-GeV bin about the $\rho_{\bar{U}U}$ are

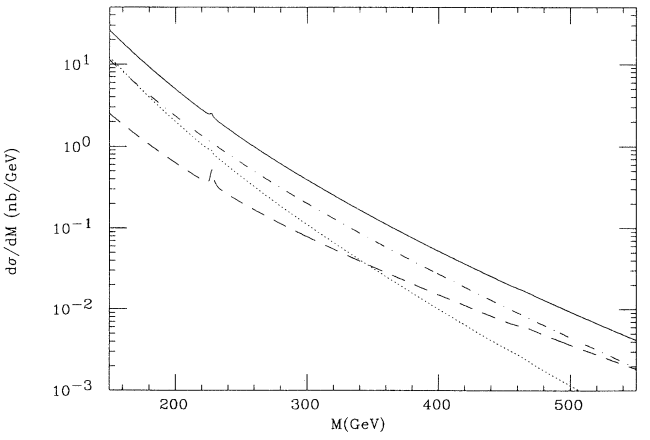

FIG. 6. The unsmeared dijet invariant-mass distribution for $\bar{p}p$ collisions at $\sqrt{s}=1800$ GeV. Both jets have rapidity $|y|<2.5$. The curves are labeled as in Fig. 1.

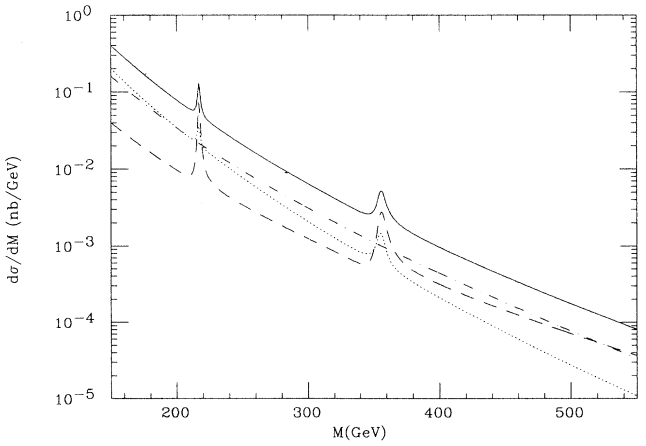

FIG. 7. The dijet invariant-mass distribution for $\bar{p}p$ collisions at $\sqrt{s}=1800$ GeV. Input masses from Eq. (4.7) were used. Both jets have rapidity $|y|<0.7$. The curves are labeled as in Fig. 1.

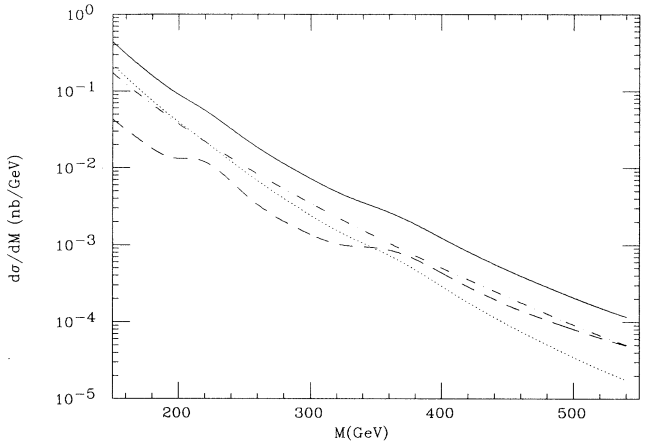

FIG. 8. The dijet invariant-mass distribution for $\bar{p}p$ collisions at $\sqrt{s}=1800$ GeV assuming a resolution of $\Delta\mathcal{M}/\mathcal{M}=0.1$. Input masses from Eq. (4.7) were used. Both jets have rapidity $|y|<0.07$. The curves are labeled as in Fig. 1.

$$\sigma_{\rho_{\bar{D}D}}(\mathrm{S}\bar{p}p\mathrm{S})=21\ \mathrm{pb},\quad \sigma_{\mathrm{bkgd}}(\mathrm{S}\bar{p}p\mathrm{S})=7\ \mathrm{pb}\ ,$$
$$\sigma_{\rho_{\bar{D}D}}(\mathrm{LHC})=29\ \mathrm{nb},\quad \sigma_{\mathrm{bkgd}}(\mathrm{LHC})=19\ \mathrm{nb}\ ,$$
$$\sigma_{\rho_{\bar{D}D}}(\mathrm{SSC})=85\ \mathrm{nb},\quad \sigma_{\mathrm{bkgd}}(\mathrm{SSC})=55\ \mathrm{nb}\ , \tag{4.8}$$
$$\sigma_{\rho_{\bar{U}U}}(\mathrm{LHC})=1.5\ \mathrm{nb},\quad \sigma_{\mathrm{bkgd}}(\mathrm{LHC})=1.4\ \mathrm{nb}\ ,$$
$$\sigma_{\rho_{\bar{U}U}}(\mathrm{SSC})=5.3\ \mathrm{nb},\quad \sigma_{\mathrm{bkgd}}(\mathrm{SSC})=4.8\ \mathrm{nb}\ .$$

Although S/B has deteriorated for LHC and SSC because of the increased importance of $\mathcal{G}\mathcal{G}$ jets, the statistical significance of the $\rho_{\bar{D}D}$ resonance at the LHC and SSC should be substantial. With the improved jet energy resolution expected for detectors at the SSC, we are confident that $\rho_{\bar{D}D}$ and $\rho_{\bar{U}U}$ can be seen in experiments there, even if they cannot be discerned at the Fermilab Tevatron.

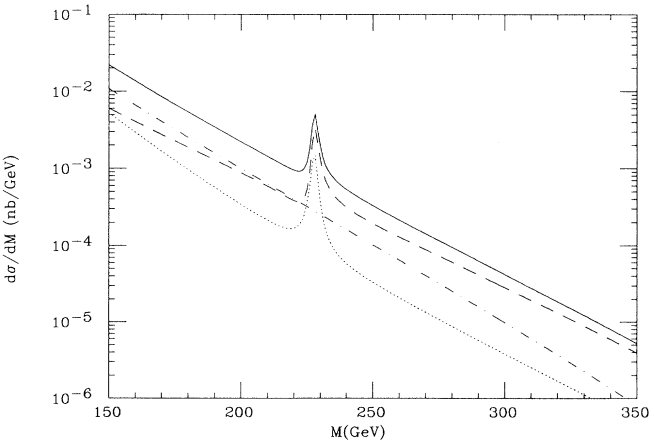

FIG. 9. The dijet invariant-mass distribution for $\bar{p}p$ collisions at $\sqrt{s}=630$ GeV. Set-A input masses were used. Both jets have rapidity $|y|<0.7$. The curves are labeled as in Fig. 1.

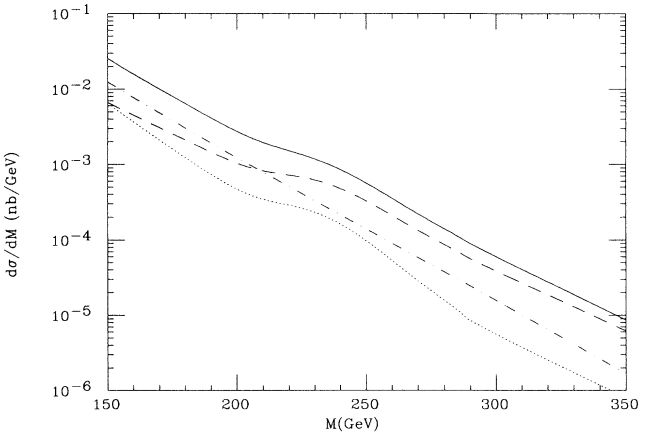

FIG. 10. The dijet invariant-mass distribution for $\bar{p}p$ collisions at $\sqrt{s}=630$ GeV assuming a resolution of $\Delta\mathcal{M}/\mathcal{M}=0.1$. Set-A input masses were used. Both jets have rapidity $|y|<0.7$. The curves are labeled as in Fig. 1.

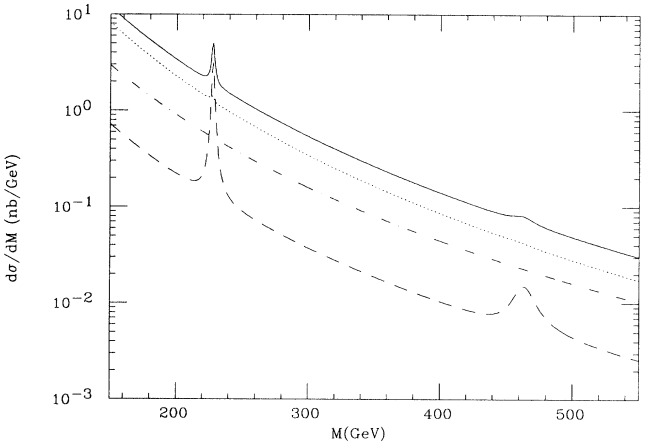

FIG. 11. The dijet invariant-mass distribution for pp collisions at $\sqrt{s}=17$ TeV. Set-A input masses were used. Both jets have rapidity $|y|<0.7$. The curves are labeled as in Fig. 1.

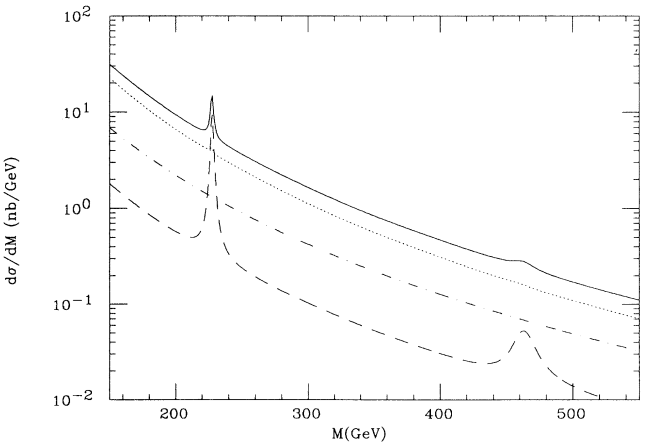

FIG. 12. The dijet invariant-mass distribution for pp collisions at $\sqrt{s}=40$ TeV. Set-A input masses were used. Both jets have rapidity $|y|<0.7$. The curves are labeled as in Fig. 1.

Colored technipion pair production at the Tevatron is displayed in Fig. 13. The cut on the π_T rapidities is $Y=0.7$. We shall discuss this cut shortly. The $\rho_{\bar{U}U}$ resonance at 465 GeV has a total width of about 20 GeV, of which about 15 GeV is to technipions. The largest contributions to the cross section come from $\pi_{\bar{D}E}\pi_{\bar{E}D}$, $\pi_{\bar{U}E}\pi_{\bar{E}U}$, $\pi_{\bar{D}D}\pi_{\bar{D}D}$, and $\pi_{\bar{D}N}\pi_{\bar{N}D}$. Because of the small mixing angle, $\gamma_W \cong 0.2$, the potentially very interesting $W^+\pi_{\bar{U}D}+W^-\pi_{\bar{D}U}$ channel has much too small a cross section to be seen above the ordinary $W^\pm$ plus two-jet background. The main $\rho_{\bar{U}U}$ decay channels are shown in Fig. 14. The integrated cross sections for these exclusive channels are

$$\begin{aligned}
&\sigma_{\pi_{\bar{D}E}\pi_{\bar{E}D}}(\text{Tevatron})=31 \text{ pb} ,\\
&\sigma_{\pi_{\bar{U}E}\pi_{\bar{E}U}}(\text{Tevatron})=21 \text{ pb} ,\\
&\sigma_{\pi_{\bar{D}D}\pi_{\bar{D}D}}(\text{Tevatron})=6.3 \text{ pb} ,\\
&\sigma_{\pi_{\bar{D}N}\pi_{\bar{N}D}}(\text{Tevatron})=2.1 \text{ pb} .
\end{aligned} \tag{4.9}$$

Several features of these production rates deserve comment.

(1) It is evident from the shape of the $\pi_{\bar{D}E}\pi_{\bar{E}D}$ and $\pi_{\bar{D}D}\pi_{\bar{D}D}$ distributions that the $\rho_{\bar{U}U}$ resonance contains a small, but non-negligible, $\bar{D}D$ component—ideal mixing is not complete. The relative sizes of the three leptoquark production rates are then due to this $\bar{D}D$ admixture, to the phase space available for each channel at the resonance, and to the appreciable continuum production of $\pi_{\bar{D}E}\pi_{\bar{E}D}$ below the resonance.

(2) The overall magnitude of leptoquark-pair production relative to octet pairs is due in part to the large number of technilepton flavors, $N_L=6$, whose splitting was *not* included in our assumed pattern of ETC breaking. As a rough measure of the effect of N_L on the cross sections, we have also computed the $\pi_T\pi_T$ rates for the *same* Set A masses with $N_L=3$. (This calculation is unjustified within our model because $\beta_{\rm TC}$, γ_{m_i}, and all the fundamental scales and masses depend on N_L.) The $\rho_{\bar{U}U}$ in this case is somewhat narrower, with a width of about 15 GeV. The π_T production rates are $\sigma_{\pi_{\bar{D}E}\pi_{\bar{E}D}}=18$ pb, $\sigma_{\pi_{\bar{U}E}\pi_{\bar{E}D}}=16$ pb, $\sigma_{\pi_{\bar{D}D}\pi_{\bar{D}D}}=8$ pb, and $\sigma_{\pi_{\bar{D}N}\pi_{\bar{N}D}}=1.5$ pb. The decrease in the leptoquark rates is due to the smaller $\mathcal{S}_{BC}=N_L$ in the numerator of their cross sections [Eqs. (3.14) and (3.16)], and this is most effective for $\pi_{\bar{D}E}\pi_{\bar{E}D}$ because of the large continuum component of its production rate. The increase in $\sigma_{\pi_{\bar{D}D}\pi_{\bar{D}D}}$ is due to the smaller $\rho_{\bar{U}U}$ width in the denominator of the cross section. We can only guess what effect splitting the technilepton masses would have on the production rates. Such a splitting would be induced by a complicated SU(N_L) asymmetric mass matrix for the relevant ETC gauge bosons. If, to avoid unwanted flavor-changing neutral currents, the lowest eigenvalues of this mass matrix must be at least 100 TeV, then the leptoquark masses in (4.1) represent an upper bound on $M_{\pi_{\bar{Q}L}}$. Then, some $\pi_{\bar{Q}L}\pi_{\bar{L}Q}$ thresholds would open up below 320 GeV and would lead to larger continuum production rates for the leptoquarks and, perhaps, a broader $\rho_{\bar{U}U}$ (and, possibly, $\rho_{\bar{D}D}$) resonance.

(3) Our cut of $Y=0.7$ on π_T rapidities is a crude guess of what may be appropriate for the CDF and D0 detectors. This is a cut on the real rapidity of the π_T's and it translates to a larger pseudorapidity which may be unrealistically large. If we follow the "conventional wisdom" for π_T decays, we expect

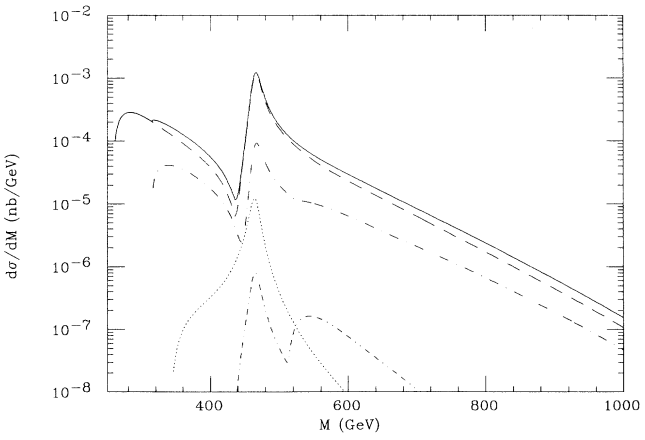

FIG. 13. The total invariant-mass distribution in technipion pair production for $\bar{p}p$ collisions at $\sqrt{s}=1800$ GeV (solid curve). Set-A input masses were used and cross sections calculated using the EHLQ Set-1 distribution functions with $Q^2=\mathcal{M}^2$. Both π_T have rapidity $|y|<0.7$. The $\pi_{\bar{Q}L}\pi_{\bar{L}Q}$ (dashed curve), $\pi_{\bar{Q}Q}\pi_{\bar{Q}Q}$ (dashed-dotted curve), $W^+\pi_{\bar{U}D}$, $W^-\pi_{\bar{D}U}$ (dotted curve), and $P_i^+\pi_{\bar{U}D}$, $P_i^-\pi_{\bar{D}U}$ (double dashed-dotted curve) channels are shown separately.

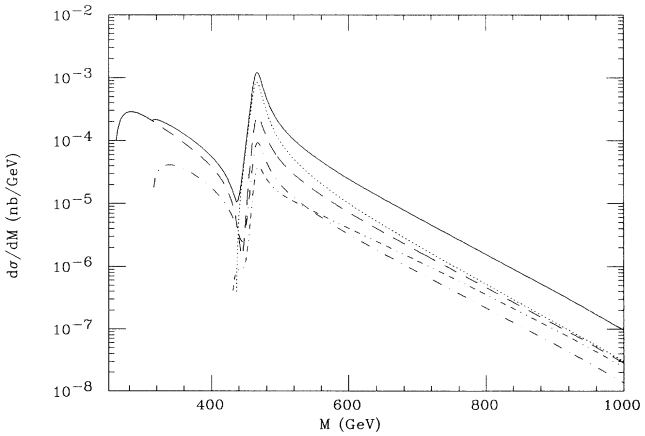

FIG. 14. The largest components of the $\pi_T\pi_T$ invariant-mass distribution for $\bar{p}p$ collisions at $\sqrt{s}=1800$ GeV. Set-A input masses were used. Both π_T have rapidity $|y|<0.7$. The channels are $\pi_{\bar{D}E}\pi_{\bar{E}D}$ (dashed curve), $\pi_{\bar{U}E}\pi_{\bar{E}U}$ (dotted curve), $\pi_{\bar{D}D}\pi_{\bar{D}D}$ (dashed-dotted curve), and $\pi_{\bar{D}N}\pi_{\bar{N}D}$ (double dashed-dotted curve). The sum of these channels is the solid curve.

$$\pi_{\bar{D}E}\to\bar{b}\tau^-,\quad \pi_{\bar{D}N}\to\bar{b}\nu\ ,$$
$$\pi_{\bar{U}E}\to\bar{t}\tau^-,\quad \pi_{\bar{D}D}\to\bar{b}b\ . \tag{4.10}$$

The light fermions into which the π_T decay each have a mobility of ~ 1 unit of rapidity and may fall outside the detectors' fiducial volumes. Furthermore, the fiducial volume of CDF (and D0 and other detectors) varies for detection of multijet events and of events with jets plus electrons and/or muons. Thus, determining a reasonable cut on the π_T rapidities appropriate to CDF and D0 is complicated and beyond the scope of the calculations in this paper.

One measure of the effect of cuts on the decay fermions is this: Chivukula, Golden, and Simmons have studied the signal and four-jet background (at the parton level) for production of a color-octet pair such as $\pi_{\bar{D}D}\pi_{\bar{D}D}$ [26]. Their signal cross section does *not* include the $\rho_{\bar{U}U}$ resonance. The signal and background are determined by pairing jets and finding the two pairs which have the closest invariant mass. We have used their routines, putting the following cuts on the four jets, designed to enhance the signal-to-background ratio and ensure separability of the jets:

$$|\mathcal{M}_{ab}-\mathcal{M}_{cd}|<10\ \text{GeV}\ ,$$
$$p_{T_a}>50\ \text{GeV}\ ,$$
$$|y_a|<0.7\ , \tag{4.11}$$
$$\sqrt{(y_a-y_b)^2+(\phi_a-\phi_b)^2}>0.7\ .$$

Following [26], we plotted the surviving cross sections against the average dijet mass $\overline{\mathcal{M}}_{jj}$ of the most equal-mass pairs. Assuming 10-GeV bins for the $\overline{\mathcal{M}}_{jj}$ data, a neutral color-octet $\pi_{\bar{D}D}$ with mass $M_{\pi_{\bar{D}D}}=160$ GeV gave a signal of only 0.1 pb above a background of 0.5 pb. Our cuts tend to select events from a region of $\pi_{\bar{D}D}$-pair invariant mass where the continuum cross section is much smaller than it is near threshold. Thus, the four-jet signal rate may be considerably larger when the technirho is included, even though it accounts for at most one-half the $\pi_{\bar{D}D}\pi_{\bar{D}D}$ production rate. Another hopeful development is that, in its next run, CDF will have a vertex detector that can be used to tag events with a b jet. Since CDF can observe and measure jets with $y\lesssim 3.5$ [24], this upgraded detector may make it possible for a larger fraction of signal events to be accepted while the background is reduced to such processes as $\mathcal{G}\mathcal{G}\bar{b}b$. Nevertheless, to observe or exclude convincingly a $\pi_{\bar{D}D}\pi_{\bar{D}D}$ signal of the size we expect here may require a luminosity above 100 pb^{-1}.

The situation may be better for leptoquarks decaying to a b jet plus a lepton. If the lepton is a τ, it will appear as a low-multiplicity jet or as a reasonably well-isolated e or μ. A detailed study of the acceptance of such events in CDF and D0, and of the backgrounds (from $Z^0\to l^+l^-$ plus two jets, $\bar{t}t$ production, etc.), is needed. While we are unaware of any such studies specific to the search for leptoquarks, they might be similar to those for the background to $\bar{t}t$ production in which both t quarks decay semileptonically.

Finally, we display the technipion production rates in the LHC and SSC. In these cases, we suppose that the detectors will have larger acceptances for jets, electrons, and muons than CDF and D0, so we assume a rapidity cut on the π_T of $Y=1.5$. The major pair production rates are shown for the LHC in Fig. 15. The exclusive channel cross sections are

$$\sigma_{\pi_{\bar{D}E}\pi_{\bar{E}D}}(\text{LHC})=5.7\ \text{nb}\ ,$$
$$\sigma_{\pi_{\bar{U}E}\pi_{\bar{E}U}}(\text{LHC})=3.6\ \text{nb}\ ,$$
$$\sigma_{\pi_{\bar{D}D}\pi_{\bar{D}D}}(\text{LHC})=2.9\ \text{nb}\ , \tag{4.12}$$
$$\sigma_{\pi_{\bar{D}N}\pi_{\bar{N}D}}(\text{LHC})=0.7\ \text{nb}\ .$$

The corresponding curves for π_T production at the SSC are shown in Fig. 16. The exclusive channel cross sections at the SSC are approximately four times larger than at the LHC:

$$\sigma_{\pi_{\bar{D}E}\pi_{\bar{E}D}}(\text{SSC})=20\ \text{nb}\ ,$$
$$\sigma_{\pi_{\bar{U}E}\pi_{\bar{E}U}}(\text{SSC})=14\ \text{nb}\ ,$$
$$\sigma_{\pi_{\bar{D}D}\pi_{\bar{D}D}}(\text{SSC})=11\ \text{nb}\ , \tag{4.13}$$
$$\sigma_{\pi_{\bar{D}N}\pi_{\bar{N}D}}(\text{SSC})=2.8\ \text{nb}\ .$$

The four-jet signals and backgrounds for $\pi_{\bar{D}D}\pi_{\bar{D}D}$ at the LHC and SSC were estimated using the routines developed in [26]. In this case, we used the following cuts on the jets:

$$|\mathcal{M}_{ab}-\mathcal{M}_{cd}|<25\ \text{GeV}\ ,$$
$$p_{T_a}>100\ \text{GeV}\ ,$$
$$|y_a|<2.0\ , \tag{4.14}$$
$$\sqrt{(y_a-y_b)^2+(\phi_a-\phi_b)^2}>1.0\ .$$

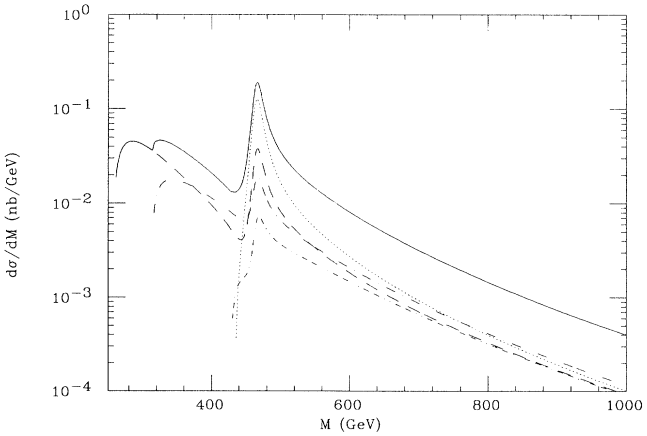

FIG. 15. The largest components of the $\pi_T\pi_T$ invariant-mass distribution for pp collisions at $\sqrt{s}=17$ TeV. Set-A masses were used. Both π_T have rapidity $|y|<1.5$. The curves are labeled as in Fig. 14.

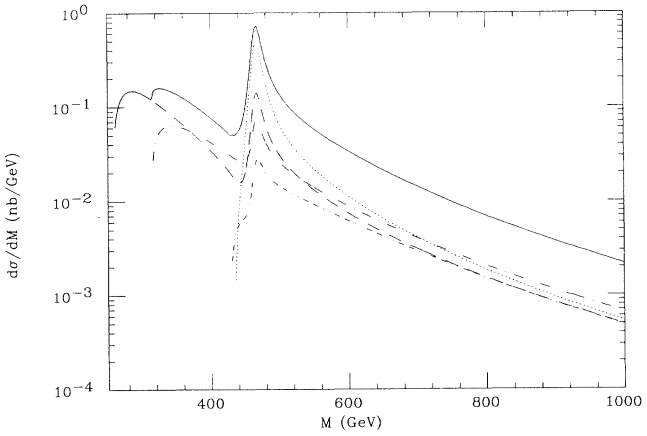

FIG. 16. The largest components of the $\pi_T\pi_T$ invariant-mass distribution for pp collisions at $\sqrt{s}=40$ TeV. Set-A masses were used. Both π_T have rapidity $|y|<1.5$. The curves are labeled as in Fig. 14.

Assuming 25-GeV bins for the $\overline{\mathcal{M}}_{jj}$ data, we obtain a signal of 10 pb and a background of 40 pb at the LHC. At the SSC, the signal and background rates are 40 pb and 140 pb. While more careful studies are needed, it appears that these technipion signals will be accessible at the LHC and the SSC even without flavor tagging.

B. Set B parameters

The Set B technihadron masses (in GeV) and the mixing factors for $W^+\pi_{\bar{U}D}$ and $P_i^+\pi_{\bar{U}D}$ production are

$$\begin{aligned} &M_{00}=484,\quad M_{11}=460,\quad M_{01}=78\ ,\\ &M_W=80,\quad M_{P_1^+}=218,\quad M_{P_2^+}=311\ ,\\ &M_{\pi_{\bar{D}U}}=318,\quad M_{\pi_{\bar{U}U}}=405,\quad M_{\pi_{\bar{D}D}}=197\ ,\\ &M_{\pi_{\bar{N}U}}=340,\quad M_{\pi_{\bar{E}U}}=265\ ,\\ &M_{\pi_{\bar{N}D}}=263,\quad M_{\pi_{\bar{E}D}}=158\ ,\\ &\gamma_W=0.301,\quad \gamma_{P_1}=0.263,\quad \gamma_{P_2}=0.917\ . \end{aligned} \tag{4.15}$$

As in Case A, the ρ_8^I appear as nearly ideally mixed resonances $\rho_{\bar{D}D}$ and $\rho_{\bar{U}U}$. Their masses and total widths are given by

$$\begin{aligned} &M_{\rho_{\bar{D}D}}\cong 400\text{ GeV},\quad \Gamma_{\rho_{\bar{D}D}}\cong 40\text{ GeV}\ ,\\ &M_{\rho_{\bar{U}U}}\cong 575\text{ GeV},\quad \Gamma_{\rho_{\bar{U}U}}\cong 20\text{ GeV}\ . \end{aligned} \tag{4.16}$$

The $\rho_{\bar{D}D}$ is above the $\pi_{\bar{D}E}\pi_{\bar{E}D}$ threshold. This accounts for most of its relatively large width and a quite different phenomenology than we found for the set A parameters.

The dijet decay rates of these resonances are $\Gamma(\rho_{\bar{D}D}\to\bar{q}q+\mathcal{G}\mathcal{G})\simeq 4.2$ GeV and $\Gamma(\rho_{\bar{U}U}\to\bar{q}q+\mathcal{G}\mathcal{G})\simeq 5.5$ GeV. Thus, we expect that, at best, only $\rho_{\bar{U}U}$ will appear in the dijet spectrum. This is borne out in Figs. 17–19 which show the *unsmeared* dijet mass distribution at the

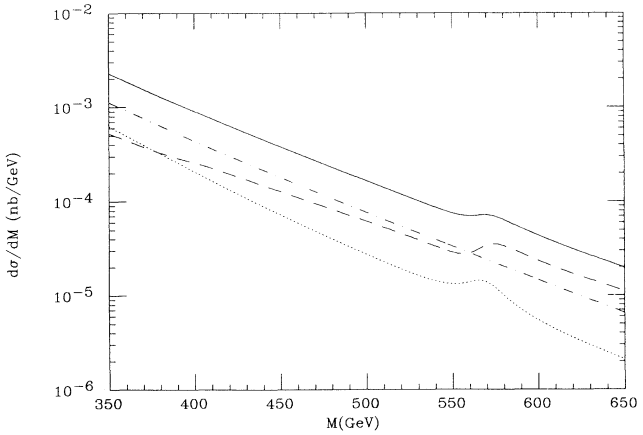

FIG. 17. The dijet invariant-mass distribution for $\bar{p}p$ collisions at $\sqrt{s}=1800$ GeV (solid curve). Set-B input masses were used and cross sections calculated using the EHLQ Set-1 distribution functions with $Q^2=\mathcal{M}^2$. Both jets have rapidity $|y|<0.7$. The qq (dashed), $\mathcal{G}\mathcal{G}$ (dotted), and $q\mathcal{G}$ (dashed-dotted) components are shown separately.

Tevatron, LHC, and SSC with a rapidity cut of $Y=0.7$. The total dijet background is also displayed in these figures. No sign of the $\rho_{\bar{D}D}$ is visible. The integrals over the $\rho_{\bar{U}U}$ from 560 to 600 GeV and the corresponding backgrounds are

$$\begin{aligned} &\sigma_{\rho_{\bar{U}U}}(\text{Tevatron})=2.5\text{ pb},\quad \sigma_{\text{bkgd}}(\text{Tevatron})=2.0\text{ pb}\ ,\\ &\sigma_{\rho_{\bar{U}U}}(\text{LHC})=0.99\text{ nb},\quad \sigma_{\text{bkgd}}(\text{LHC})=0.93\text{ nb}\ ,\\ &\sigma_{\rho_{\bar{U}U}}(\text{SSC})=3.7\text{ nb},\quad \sigma_{\text{bkgd}}(\text{SSC})=3.5\text{ nb}\ . \end{aligned} \tag{4.17}$$

Although S/B is best at the Tevatron (where $\bar{q}q$ annihilation dominates the jet cross section above $\mathcal{M}\simeq 500$ GeV), the $\rho_{\bar{U}U}$ will be out of reach there until the luminosity exceeds 100 pb^{-1}, and perhaps, even then. It will be very

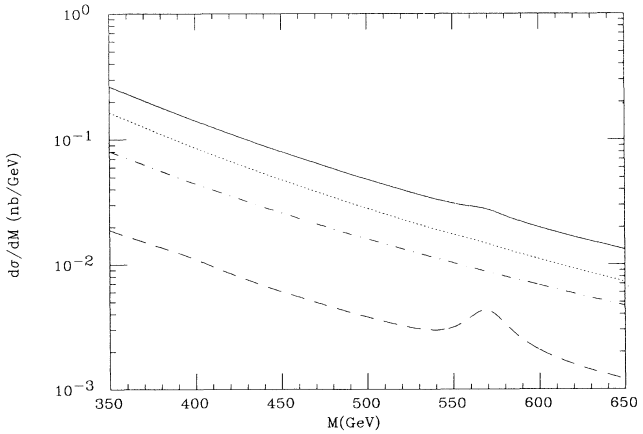

FIG. 18. The dijet invariant-mass distribution for pp collisions at $\sqrt{s}=17$ TeV. Set-B input masses were used. Both jets have rapidity $|y|<0.7$. The curves are labeled as in Fig. 17.

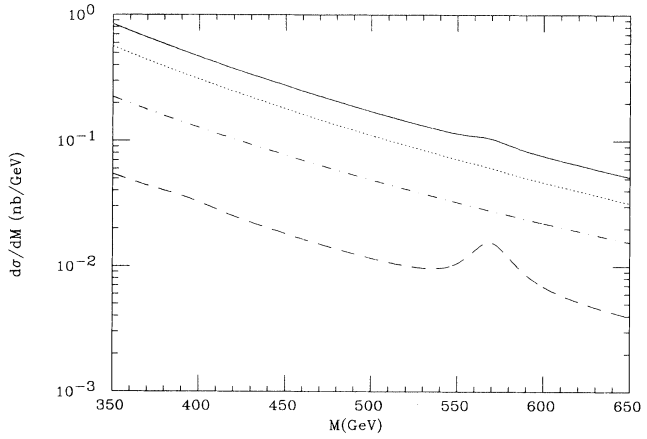

FIG. 19. The dijet invariant-mass distribution for pp collisions at $\sqrt{s}=40$ TeV. Set-B input masses were used. Both jets have rapidity $|y|<0.7$. The curves are labeled as in Fig. 17.

difficult to observe this $\rho_{\bar{U}U}$ at LHC and SSC unless the dijet mass resolution is 5% or better *and* it is possible to distinguish quark jets from gluon jets.

The inclusive technipion pair production rates at the Tevatron are shown in Fig. 20. Again, we have chosen a rapidity cut of $Y=0.7$. The major decay modes of the $\rho_{\bar{Q}Q}$ resonances are

$$\rho_{\bar{D}D}\to\pi_{\bar{D}E}\pi_{\bar{E}D},\quad \rho_{\bar{U}U}\to\pi_{\bar{U}E}\pi_{\bar{E}U}\ ,$$
$$\pi_{\bar{D}E}\pi_{\bar{E}D},\quad \pi_{\bar{D}D}\pi_{\bar{D}D},\quad \pi_{\bar{D}N}\pi_{\bar{N}D}\ . \tag{4.18}$$

The integrated cross sections for these channels are (see Fig. 21)

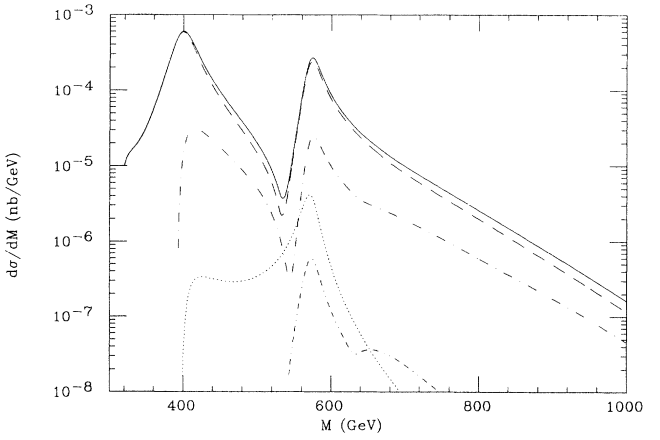

FIG. 20. The total invariant-mass distribution in technipion pair production for $\bar{p}p$ collisions at $\sqrt{s}=1800$ GeV (solid curve). Set-B input masses were used and cross sections calculated using the EHLQ Set-1 distribution functions with $Q^2=\mathcal{M}^2$. Both π_T have rapidity $|y|<0.7$. The $\pi_{\bar{Q}L}\pi_{\bar{L}Q}$ (dashed curve), $\pi_{\bar{Q}Q}\pi_{\bar{Q}Q}$ (dashed-dotted curve), $W^+\pi_{\bar{U}D}$, $W^-\pi_{\bar{D}U}$ (dotted curve), and $P_i^+\pi_{\bar{U}D}$, $P_i^-\pi_{\bar{D}U}$ (double dashed-dotted curve) channels are shown separately.

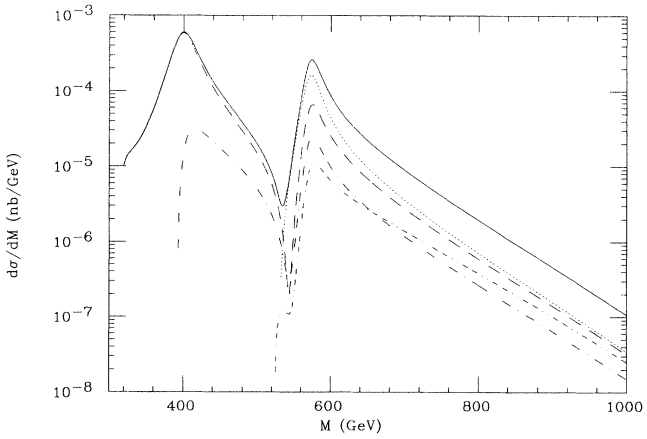

FIG. 21. The largest components of the $\pi_T\pi_T$ invariant-mass distribution for $\bar{p}p$ collisions at $\sqrt{s}=1800$ GeV. Set-B input masses were used. Both π_T have rapidity $|y|<0.7$. The channels are $\pi_{\bar{D}E}\pi_{\bar{E}D}$ (dashed curve), $\pi_{\bar{U}E}\pi_{\bar{E}U}$ (dotted curve), $\pi_{\bar{D}D}\pi_{\bar{D}D}$ (dashed-dotted curve), and $\pi_{\bar{D}N}\pi_{\bar{N}D}$ (double dashed-dotted curve). The sum of these channels is the solid curve.

$$\begin{aligned}
&\sigma_{\pi_{\bar{D}E}\pi_{\bar{E}D}}(\text{Tevatron})=30\text{ pb}\ ,\\
&\sigma_{\pi_{\bar{U}E}\pi_{\bar{E}U}}(\text{Tevatron})=6.1\text{ pb}\ ,\\
&\sigma_{\pi_{\bar{D}D}\pi_{\bar{D}D}}(\text{Tevatron})=3.0\text{ pb}\ ,\\
&\sigma_{\pi_{\bar{D}N}\pi_{\bar{N}D}}(\text{Tevatron})=0.7\text{ pb}\ .
\end{aligned} \tag{4.19}$$

We see in Fig. 21 that most of the $\pi_{\bar{D}E}\pi_{\bar{E}D}$ production comes from the $\rho_{\bar{D}D}$ resonance. Compared to Case A [see (4.9)], all of the other channels have production rates which are smaller by a factor of 2–3. This occurs because of the larger technihadron masses in (4.15), a consequence, ultimately, of the scaling assumption B in (2.20). The bulk of the $\pi_{\bar{D}D}\pi_{\bar{D}D}$ production comes from the continuum just above (and modified by) the $\rho_{\bar{D}D}$ resonance. Most of the remarks made in Case A regarding the dependence of these cross sections on model assumptions and the observability of specific final states apply here. One difference is that the production rates computed with the same masses, but $N_L=3$, are essentially unchanged from those in (4.19); in particular, we again find $\sigma_{\pi_{\bar{D}E}\pi_{\bar{E}D}}(\text{Tevatron})=30$ pb. The reason for this is that the $\rho_{\bar{D}D}$ decays almost entirely to $\pi_{\bar{D}E}\pi_{\bar{E}D}$, and so, the integral over the resonance is almost independent of N_L. Using the cuts in (4.11), we find that the signal for pair production of a 200-GeV $\pi_{\bar{D}D}$ is 0.02 pb with a background of 0.15 pb. If this result holds under more careful study (including the $\rho_{\bar{U}U}$ resonance), flavor tagging would be essential to searching for this $\pi_{\bar{D}D}$ at the Tevatron.

The large components of technipion pair production rates are shown in Fig. 22 for the LHC. As in Case A, a rapidity cut of $Y=1.5$ is imposed on the π_T. The principal exclusive channel cross sections are

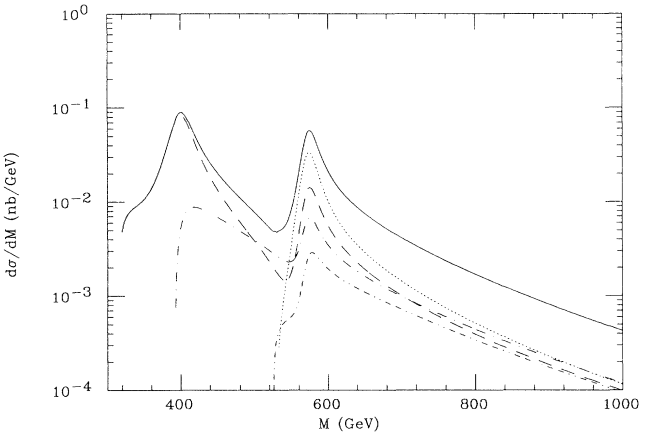

FIG. 22. The largest components of the $\pi_T\pi_T$ invariant-mass distribution for pp collisions at $\sqrt{s}=17$ TeV. Set-B masses were used. Both π_T have rapidity $|y|<1.5$. The curves are labeled as in Fig. 21.

$$\begin{aligned}
&\sigma_{\pi_{\bar{D}E}\pi_{\bar{E}D}}(\mathrm{LHC})=5.3\ \mathrm{nb}\ ,\\
&\sigma_{\pi_{\bar{U}E}\pi_{\bar{E}U}}(\mathrm{LHC})=1.5\ \mathrm{nb}\ ,\\
&\sigma_{\pi_{\bar{D}D}\pi_{\bar{D}D}}(\mathrm{LHC})=1.3\ \mathrm{nb}\ ,\\
&\sigma_{\pi_{\bar{D}N}\pi_{\bar{N}D}}(\mathrm{LHC})=0.3\ \mathrm{nb}\ .
\end{aligned} \tag{4.20}$$

The corresponding curves for π_T production at the SSC are shown in Fig. 23. Here again, the principal exclusive channel cross sections are about four times larger than those at the LHC:

$$\begin{aligned}
&\sigma_{\pi_{\bar{D}E}\pi_{\bar{E}D}}(\mathrm{SSC})=19\ \mathrm{nb}\ ,\\
&\sigma_{\pi_{\bar{U}E}\pi_{\bar{E}U}}(\mathrm{SSC})=6.1\ \mathrm{nb}\ ,\\
&\sigma_{\pi_{\bar{D}D}\pi_{\bar{D}D}}(\mathrm{SSC})=5.5\ \mathrm{nb}\ ,\\
&\sigma_{\pi_{\bar{D}N}\pi_{\bar{N}D}}(\mathrm{SSC})=1.4\ \mathrm{nb}\ .
\end{aligned} \tag{4.21}$$

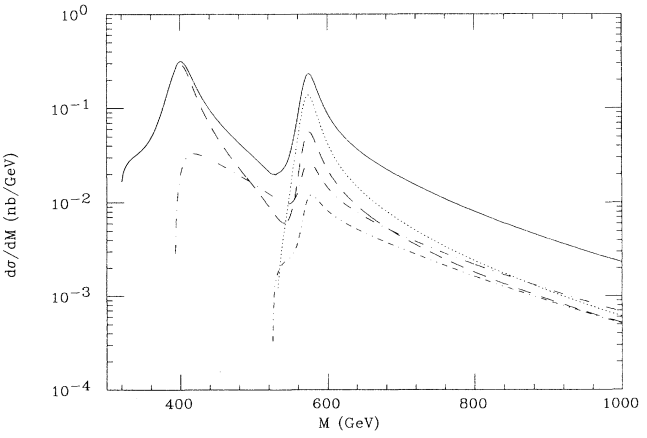

FIG. 23. The largest components of the $\pi_T\pi_T$ invariant-mass distribution for pp collisions at $\sqrt{s}=40$ TeV. Set-B masses were used. Both π_T have rapidity $|y|<1.5$. The curves are labeled as in Fig. 21.

Following [26], with the cuts in (4.14), we estimate the $\pi_{\bar{D}D}\pi_{\bar{D}D}\to$four jets signal and background rates to be 15 pb and 55 pb at the LHC, 65 pb and 190 pb at the SSC. With such large cross sections, it seems very likely that the $\pi_{\bar{D}D}$ signal will be accessible at the LHC and SSC even if it is not at the Tevatron. Nevertheless, color-octet, as well as leptoquark, signal and background rates deserve more careful study.

C. Summary

Walking technicolor is so far the only dynamical picture of electroweak- and flavor-symmetry breaking that seems able to eliminate unwanted flavor-changing neutral-current interactions. If the walking coupling is realized by having technifermions in both fundamental and higher-dimensional representations of the technicolor gauge group, then there will be several scales of chiral-symmetry breaking with the largest (highest-dimension) scale pinned down by the electroweak energy of 1 TeV. It is then plausible that the lowest scale is in the energy range covered by the Tevatron, and if this scale belongs to colored techniquarks, the corresponding technihadrons ρ_T and π_T will be copiously produced there. The mass enhancements characteristic of walking technicolor tend to raise $2M_{\pi_T}$ relative to M_{ρ_T}, closing off many, if not all, of the $\rho_T\to\pi_T\pi_T$ decay channels. Thus, it is possible that some ρ_T will be quite narrow, decaying predominantly to dijets, an important and simple final state. Those that decay to $\pi_T\pi_T$ will have only a few important channels and will also be relatively narrow compared to expectations in nonwalking models of technicolor [1]. Finally, the large weak isospin splitting that must be present in walking technicolor models if they are to explain the t-b mass difference implies that neutral, color-octet (and singlet) ρ_T will be nearly ideally mixed, well-separated $\rho_{\bar{D}D}$ and $\rho_{\bar{U}U}$ resonances in dijet and $\pi_T\pi_T$ production. The rates for these processes at hadron colliders are effectively of $O(\alpha_{\mathrm{QCD}}^2)$ and, up to questions of resolution, acceptance, and background, most of them may be observable at the Tevatron for $M_{\rho_{\bar{Q}Q}}\sim 200$–$600$ GeV.

These expectations were realized and illustrated in an explicit multiscale model of walking technicolor. The light-scale technifermions in this model consist of one electroweak doublet of techniquarks and $N_L=6$ doublets of technileptons, all belonging to the fundamental representation of SU(N_{TC}). The colored technihadrons of interest are color-octet technirhos ($\rho_{\bar{D}D}$ and $\rho_{\bar{U}U}$) and color-octet ($\pi_{\bar{Q}Q}$) and -triplet ($\pi_{\bar{L}Q}$ and $\pi_{\bar{Q}L}$) technipions. Forced by our basic ignorance of how to estimate fundamental parameters in a walking gauge theory, we considered two QCD-motivated schemes, A and B, for calculating Λ_i/F_i and $\langle\bar{T}_iT_i\rangle$ [see (2.20) and (2.24)]. These schemes led to quite different technihadron spectra and decay patterns, but in both cases, the ρ_T and π_T could be within reach of experiments at the Tevatron, and certainly within the reach of those at the LHC and SSC.

In scheme A, we typically found $M_{\rho_{\bar{D}D}}=200$–250 GeV

and $M_{\rho_{\bar{U}U}}=350-550$ GeV. For a reasonable range of our adjustable parameters, the $\pi_T\pi_T$ decay channels of $\rho_{\bar{D}D}$ are closed, so that it appears as a narrow resonance in dijet production at the Tevatron with a signal cross section of 100–300 pb. With a 10% dijet mass resolution, this signal is 5–10 times smaller than the background. To see this signal, it is important that a relatively tight rapidity cut is made on the dijets to enhance the dominant and central $\bar{q}q$ signal over the $\mathcal{G}\mathcal{G}$ and $q\mathcal{G}$ dijets. Obviously, it would be very useful if quark jets and gluon jets can be discriminated with reasonable efficiency. We are reasonably confident that the dijet signal for $\rho_{\bar{D}D}$ can be seen at the SSC (and LHC) because the signal rate is enormous and the detectors are expected to have better resolution. Ideal mixing is not complete and the $\rho_{\bar{U}U}$ tends to be far enough above several $\pi_T\pi_T$ thresholds, specifically $\pi_{\bar{D}E}\pi_{\bar{E}D}$, $\pi_{\bar{U}E}\pi_{\bar{E}U}$, and $\pi_{\bar{D}D}\pi_{\bar{D}D}$, that these modes are its dominant production signals. These technipions conventionally are expected to decay as $\pi_{\bar{D}E}\to\bar{b}\tau^-$, $\pi_{\bar{U}E}\to\bar{t}\tau^-$, and $\pi_{\bar{D}D}\to\bar{b}b$. We found that $\rho_{\bar{U}U}\to\pi_T\pi_T$ rates at the Tevatron are each of order 10 pb, but reliable estimates of these rates will require careful, detector-specific simulations of the signals and their backgrounds. Assuming these backgrounds are not too severe, the large production rates at the SSC, and the better coverage and resolution of SSC detectors, should ensure that the color-triplets and octets can be excluded, or discovered, there.

In Scheme B, we found $M_{\rho_{\bar{D}D}}=375-425$ GeV and $M_{\rho_{\bar{U}U}}=500-700$ GeV. Both resonances were above the $\pi_T\pi_T$ threshold and tend not to be visible in dijet production *unless* it is possible to enrich the sample of dijets containing quarks. As in Case A, the rates for the $\pi_T\pi_T$ channels were naively calculated to be of order 10 pb at the Tevatron, but simulations are still needed to determine the potential for their discovery there. We expect that the technipions will be much more accessible at the SSC than at the Tevatron. At any collider, the search for the color-triplet and -octet technipions must be flexible, with different search strategies for threshold and for resonance production. Certainly, the first signal to look for is the predominance of heavy quarks and leptons in π_T decays expected in ETC models. But, it must be recognized that no satisfactory ETC model exists, and assuming one can be constructed, π_T decays may be different than we have imagined.

Finally, we return to the question of what happens if ETC interactions are so strong that they participate significantly in the breakdown of technifermion chiral symmetries [10]. For strong ETC interactions to be relevant to the scenario presented in this paper, we suppose that they affect even the light-scale technifermions of a multiscale model. The effect of strong ETC is to give such large hard masses to the technifermions that chiral perturbation theory breaks down. The π_T can no longer be regarded as pseudo-Goldstone bosons; their masses are expected to be given by the sum of their constituent technifermion masses. This is the situation that occurs in heavy-quark systems, where $M_\psi<2M_D$ and $M_\Gamma<2M_B$. Thus, we still expect to find ideally mixed $\rho_{\bar{D}D}$ and $\rho_{\bar{U}U}$ with $M_{\rho_{\bar{D}D}}<2M_{\pi_T}$. The $\rho_{\bar{D}D}$ will be very narrow and will always decay to two QCD jets. Furthermore, $\rho_{\bar{D}D}$ should still be in the Tevatron energy range because, as we have emphasized, the highest technifermion scale is constrained from above by the electroweak energy. On the other hand, weak isospin breaking can be expected to put $\rho_{\bar{U}U}$ above the $\pi_{\bar{D}E}\pi_{\bar{E}D}$ and $\pi_{\bar{D}D}\pi_{\bar{D}D}$ thresholds. Since ideal mixing probably will be imperfect, $\rho_{\bar{U}U}$ will decay to these states as well as dijets, the relative rates depending on the $\bar{D}D$ contamination in $\rho_{\bar{U}U}$. We conclude that the signatures of a multiscale model with strong ETC interactions will not be very different from what we found in Case A and, in particular, such a scenario is subject to test at the Tevatron, LHC, and SSC.

ACKNOWLEDGMENTS

We are indebted to Sekhar Chivukula, Mitchell Golden, and Elizabeth Simmons for careful readings of the manuscript and for critical comments. We also thank Estia Eichten and Howard Georgi for valuable comments. We gratefully acknowledge John Huth, Steve Geer, and other members of the CDF Collaboration for very useful discussions on aspects of the detector and its capabilities for searching for the signatures discussed in this paper. This work was supported in part by the U.S. Department of Energy under Contract No. DE-AC02-89ER40509 and by the Texas National Research Laboratory Commission under Grant No. RGFY91B6.

APPENDIX: TECHNIFERMION AND TECHNIPION MASSES

We summarize here the formulas for the masses of technifermions and technipions that occur in the multiscale ETC model of Sec. II. We remind the reader that these masses are computed assuming the validity of chiral perturbation theory. The model is based on the gauge group $G_{\rm ETC}=\mathrm{SU}(N_{\rm ETC})_1\otimes\mathrm{SU}(N_{\rm ETC})_2$ with gauge couplings g_1 and g_2. At the scale M_A, $G_{\rm ETC}$ is assumed to be broken down to $\mathrm{SU}(N_{\rm ETC})_{1+2}$ with gauge coupling $g_{\rm ETC}=g_1g_2/\sqrt{g_1^2+g_2^2}$. At the lower scale M_V, $\mathrm{SU}(N_{\rm ETC})_{1+2}$ is further broken down to $\mathrm{SU}(N_{\rm TC})\otimes\mathrm{SU}(3)\otimes\mathrm{SU}(N_L)$. The technifermions that emerge at this scale are the chiral doublets ψ, techniquarks Q, and technileptons L, transforming as in (2.2). To keep our calculations tractable, we assumed that the technilepton flavor group $\mathrm{SU}(N_L)$ was not broken. In our calculations, we took $N_{\rm TC}=N_L=6$ to ensure a walking $\alpha_{\rm TC}$ from $2\Lambda_\psi$ to M_V. The complete list of massive ETC gauge bosons that emerge in this model are

$$
\begin{aligned}
&G_{T_A}\in(\mathrm{N}_{\mathrm{TC}}^2-1,1_C,1_L),G_{C_A}\in(1_{\mathrm{TC}},8_C,1_L)\ ,\\
&G_{L_{V,A}}\in(1_{\mathrm{TC}},1_C,\mathrm{N}_L^2-1)\ ,\\
&X_{V,A}\in(\mathrm{N}_{\mathrm{TC}},3_C^*,1_L)\oplus(\mathrm{N}_{\mathrm{TC}}^*,3_C,1_L)\ ,\\
&Y_{V,A}\in(\mathrm{N}_{\mathrm{TC}},1_C,\mathrm{N}_L^*)\oplus(\mathrm{N}_{\mathrm{TC}}^*,1_C,\mathrm{N}_L)\ ,\\
&Z_{V,A}\in(1_{\mathrm{TC}},3_C,\mathrm{N}_L^*)\oplus(1_{\mathrm{TC}},3_C^*,\mathrm{N}_L)\ ,\\
&B_{1_{V,A}},B_{2_{V,A}}\in(1_{\mathrm{TC}},1_C,1_L)\ .
\end{aligned}
\tag{A1}
$$

The subscript A or V connotes that the gauge boson has mass M_A or $M_V<M_A$, respectively. The ETC bosons $B_{1_{V,A}}$ and $B_{2_{V,A}}$ couple to the various U(1) currents that arise in the breakdown of G_{ETC}.

1. Dominant contributions to technifermion hard masses

The hard masses of ψ_U and ψ_D arise from the exchange of G_{T_A} and $B_{i_{V,A}}$ bosons and are given at the scale Λ_ψ by

$$
m_{\psi_U,\psi_D}(\Lambda_\psi)=\frac{g_{\mathrm{ETC}}^2\langle\bar\psi\psi\rangle_{\Lambda_\psi}}{d_\psi M_V^2}\left[4(Y_1^2+Y_2^2)\exp\left[2\int_{\Lambda_\psi}^{M_V}\frac{d\mu}{\mu}\gamma_{m_3}(\mu)\right]\right.
$$
$$
\left.+\eta_{U,D}\frac{M_V^2}{M_A^2}[C_{2\psi}+4(Y_1^2+Y_2^2)]\exp\left[2\int_{\Lambda_\psi}^{M_A}\frac{d\mu}{\mu}\gamma_{m_3}(\mu)\right]\right]\ . \tag{A2}
$$

Here, $d_\psi=\frac{1}{2}N_{\mathrm{TC}}(N_{\mathrm{TC}}-1)$ is the dimensionality of the SU(N_{TC}) representation of ψ, $C_{2\psi}=(N_{\mathrm{TC}}-2)(N_{\mathrm{TC}}+1)/N_{\mathrm{TC}}$ is its quadratic Casimir, and

$$
Y_1=\left[\frac{N_L}{2(N_{\mathrm{TC}}+3)(N_{\mathrm{ETC}}+N_L+3)}\right]^{1/2},\qquad
Y_2=\left[\frac{3}{2N_{\mathrm{TC}}(N_{\mathrm{TC}}+3)}\right]^{1/2} \tag{A3}
$$

are the U(1) charges of ψ. Weak isospin breaking is parametrized by

$$
\eta_U=(g_1/g_2)^2,\quad \eta_D=-1\ . \tag{A4}
$$

This factor arises because up and down fermions are assigned to different representations of G_{ETC}. Note that m_{ψ_D} is negative. This does not lead to any interesting CP-violating effects in the quark sector of this model. In computing the integrals that occur in Eq. (A2) and below, we take $\gamma_{m_i}(\mu)=1$ for $\Lambda_i<\mu<2\Lambda_i$ [21] and $\gamma_{m_i}(\mu)=\gamma_{m_i}(M_V)$ for $M_V<\mu<M_A$. The factor of 2 multiplying the integrals comes from relating $\langle\bar\psi\psi\rangle_{M_{V,A}}$ to $\langle\bar\psi\psi\rangle_{\Lambda_\psi}$ and the running of the M_V, M_A components of the hard mass from $M_{V,A}$ down to Λ_ψ as dictated by (2.25).

The dominant contributions to the hard masses $m_{U,D}$ and $m_{N,E}$ come, respectively, from $X_{V,A}$- and $Y_{V,A}$-exchange graphs connecting U,D and N,E to ψ_U,ψ_D. As described in [6], there are sizable contributions to these hard masses from *both* the dynamical and hard-mass parts of the ψ propagator in the techniquark and technilepton self-energy graphs. For the U and D hard masses, we obtain

$$
m_{U,D}(\Lambda_Q)\cong g_{\mathrm{ETC}}^2\left[B_{V_{U,D}}\exp\left[\int_{\Lambda_Q}^{M_V}\frac{d\mu}{\mu}\gamma_{m_2}(\mu)\right]\right.
$$
$$
\left.+\eta_{U,D}B_{A_{U,D}}\exp\left[\int_{\Lambda_Q}^{M_A}\frac{d\mu}{\mu}\gamma_{m_2}(\mu)\right]\right], \tag{A5}
$$

where B_{V_U} is given by

$$
B_{V_U}=\frac{\langle\bar\psi\psi\rangle_{\Lambda_\psi}}{N_{\mathrm{TC}}M_V^2}\exp\left[\int_{\Lambda_\psi}^{M_V}\frac{d\mu}{\mu}\gamma_{m_3}(\mu)\right]+\frac{N_{\mathrm{TC}}-1}{4\pi^2}m_{\psi_U}(\Lambda_\psi)\int_0^{\ln M_V/\Lambda_\psi}dt\left[\frac{\exp\left[-\int_t^{\ln M_V/\Lambda_\psi}ds\,\gamma_{m_3}(s)\right]}{1+e^{2t}}\right]. \tag{A6}
$$

Corresponding expressions give B_{V_D}, B_{A_U}, and B_{A_D}. The second term in (A6) is the integral over the running hard mass of ψ. We find that it is somewhat smaller than the dynamical (first) term, which is different from what was found in [6] with cruder approximations. The technilepton hard masses $m_{N,E}(\Lambda_L)$ are obtained by making the appropriate changes in Eq. (A5).

For the model parameters $M_V=100$ TeV, $M_A=400$ TeV, $(g_1/g_2)^2=1.5$, and $\kappa=1.5$, the hard masses (in GeV) for Case A in (2.21) and (2.24) are given by

$$
\begin{aligned}
&m_{\psi_U}=223,\quad m_{\psi_D}=-133\ ,\\
&m_U=136,\quad m_D=22\ ,\\
&m_N=61,\quad m_E=13\ .
\end{aligned}
\tag{A7}
$$

For the same model parameters, the hard masses in Case B are

$$m_{\psi_U}=119,\quad m_{\psi_D}=-70\ ,$$
$$m_U=92,\quad m_D=14\ , \tag{A8}$$
$$m_N=43,\quad m_E=9\ .$$

We see in Eqs. (A4) and (A5) that up-down mass splittings grow linearly with $(g_1/g_2)^2$. From (2.24), we also see that all hard masses grow linearly with κ. It is then easy to estimate the hard masses for other values of M_A/M_V, $(g_1/g_2)^2$, and κ. The large splitting between techniquark and technilepton masses is due to the dependence of γ_{m_2} on the QCD coupling $\alpha_{\rm QCD}(\mu)$ which is growing above $\mu=\Lambda_Q$ to meet $\alpha_{\rm TC}(\mu)$ at $\mu=M_V$.

2. Technipion masses

To calculate the masses of $\pi_{\bar{Q}Q}$, $\pi_{\bar{L}Q}$, and P_i^+ in the limit $F_L\cong F_Q\ll F_\psi$, it might be thought that one could use an effective chiral-symmetry-breaking Hamiltonian, analogous to the quark-mass terms in QCD, obtained in integrating out the heavy ψ technifermions. However, this procedure fails to give the masses of $\pi_{\bar{Q}L}$ correctly because of the different scalings of $\bar{Q}Q$ and $\bar{L}L$ between M_V, M_A, and $\Lambda_Q\cong\Lambda_L$. The correct effective Hamiltonian (up to very small $\bar{Q}Q\bar{Q}Q$, $\bar{L}L\bar{L}L$, and $\bar{Q}L\bar{L}Q$ terms) is given by

$$\mathcal{H}_{\rm eff}=\frac{g_{\rm ETC}^2}{2M_V^2}(\bar{Q}_L\gamma^\mu\psi_L\bar{\psi}_R\gamma_\mu Q_R+\bar{L}_L\gamma^\mu\psi_L\bar{\psi}_R\gamma_\mu L_R+\text{H.c.})+\frac{g_{\rm ETC}^2}{2M_A^2}(\bar{Q}_L\gamma^\mu\psi_L\bar{\psi}_R\gamma_\mu\mathcal{A}Q_R+\bar{L}_L\gamma^\mu\psi_L\bar{\psi}_R\gamma_\mu\mathcal{A}L_R+\text{H.c.})$$
$$+\frac{1}{2}\int\frac{d^4k}{(2\pi)^4}g_{\rm QCD}^2(k^2)\Delta^{\mu\nu}(k)\sum_{A=1}^{8}\int d^4x\,e^{-ik\cdot x}T(\bar{Q}(x)\gamma_\mu t_A Q(x)\bar{Q}(0)\gamma_\nu t_A Q(0))\ . \tag{A9}$$

The fermion fields are written in doublet notation and $\mathcal{A}=\eta_U(1+\tau_3)/2+\eta_D(1-\tau_3)/2$ expresses the isospin breaking. Technicolor, color, and flavor indices are suppressed. The operators in the four-fermion terms are renormalized at the appropriate ETC scale, M_V or M_A. The last term in $\mathcal{H}_{\rm eff}$ is the one QCD-gluon-exchange contribution to chiral-symmetry breaking, where $\Delta_{\mu\nu}$ is the gluon propagator and t_A is the SU(3) generator of Q. In nonwalking theories of technicolor, this QCD term gave the dominant contribution to the mass of colored technipions, much larger than the ETC-generated mass terms [27,5]. Insofar as we can estimate the QCD contribution to colored-π_T masses in a walking theory, we shall see that this is no longer true.

The color-octet technipion masses are obtained from $\mathcal{H}_{\rm eff}$ as (for $Q,Q'=U,D$)

$$M^2_{\pi_{\bar{Q}Q'}}\cong\frac{1}{F_Q^2}(m_Q+m'_Q)\langle\bar{Q}Q\rangle_{\Lambda_Q}+\delta M_8^2\ , \tag{A10}$$

where masses and condensates are renormalized at Λ_Q. The authors of Ref. [27] estimated the QCD contribution δM_8^2 using the time-honored method of first writing techniquark-current correlations as integrals over spectral functions (satisfying Weinberg sum rules [28]) and then dominating the spectral integrals by the lowest-lying vector and axial-vector mesons. It is far from obvious that this procedure is valid in a walking technicolor model because of the slow falloff of the spectral functions, and, hence the slow convergence of the spectral integrals. Nevertheless, it probably is adequate for our purposes because we do not need to know δM_8^2 very precisely [29]. Then, directly copying the calculation in [27], we obtain

$$\delta M_8^2\simeq\frac{9}{4\pi}\alpha_{\rm QCD}(2\Lambda_Q)[\tfrac{1}{2}(M_{\rho_{\bar{U}U}}+M_{\rho_{\bar{D}D}})]^2\ln 2\ , \tag{A11}$$

where we took the ratio of axial-vector to vector masses to be $\sqrt{2}$. This contributes about $(65\ \text{GeV})^2$ in Case A [$(95\ \text{GeV})^2$ in Case B] to $M^2_{\pi_{\bar{Q}Q}}$, considerably less than the hard-mass terms in (A10).

The leptoquark masses are given by

$$M^2_{\pi_{\bar{D}E}}\cong\frac{1}{F_Q^2}(m_D\langle\bar{Q}Q\rangle_{\Lambda_Q}+m_E\langle\bar{L}L\rangle_{\Lambda_L})+\delta M_3^2\ ,$$
$$M^2_{\pi_{\bar{U}N}}\cong\frac{1}{F_Q^2}(m_U\langle\bar{Q}Q\rangle_{\Lambda_Q}+m_N\langle\bar{L}L\rangle_{\Lambda_L})+\delta M_3^2\ , \tag{A12}$$
$$M^2_{\pi_{\bar{D}N}}\cong M^2_{\pi_{\bar{U}E}}\cong\frac{1}{2F_Q^2}[(m_U+m_D)\langle\bar{Q}Q\rangle_{\Lambda_Q}+(m_N+m_E)\langle\bar{L}L\rangle_{\Lambda_L}]+\delta M_3^2\ ,$$

where we approximated the QCD contribution by

$$\delta M_3^2\simeq\frac{4}{4\pi}\alpha_{\rm QCD}(2\Lambda_Q)[\tfrac{1}{2}(M_{\rho_{\bar{U}U}}+M_{\rho_{\bar{E}E}})]^2\ln 2\ . \tag{A13}$$

Finally, to calculate the masses of the charged color-singlet technipions P_i^+, it is necessary to construct combinations of ψ, Q, and L chiral generators in the subspace orthogonal to the massless technipion W_L^+. When this is done, we find the obvious answer in the limit $F_Q\cong F_L\ll F_\psi$:

$$M^2_{P_1^+}\simeq\frac{1}{F_L^2}(m_N+m_E)\langle\bar{L}L\rangle_{\Lambda_L}\ ,$$
$$M^2_{P_2^+}\simeq\frac{1}{F_Q^2}(m_U+m_D)\langle\bar{Q}Q\rangle_{\Lambda_Q}\ . \tag{A14}$$

This last result is only approximate, as evidenced by the small, but nonzero values in (2.29) and (2.30) of the mixing factor γ_1 describing the $\bar{D}U$ component of P_1^+.

[1] E. Eichten, I. Hinchliffe, K. Lane, and C. Quigg, Rev. Mod. Phys. **56**, 579 (1984).

[2] E. Eichten, I. Hinchliffe, K. Lane, and C. Quigg, Phys. Rev. D **34**, 1547 (1986).

[3] B. Holdom, Phys. Rev. D **24**, 1441 (1981); Phys. Lett. **150B**, 301 (1985); T. Appelquist, D. Karabali, and L. C. R. Wijewardhana, Phys. Rev. Lett. **57**, 957 (1986); T. Appelquist and L. C. R. Wijewardhana, Phys. Rev. D **36**, 568 (1987); K. Yamawaki, M. Bando, and K. Matumoto, Phys. Rev. Lett. **56**, 1335 (1986); T. Akiba and T. Yanagida, Phys. Lett. **169B**, 432 (1986).

[4] S. Dimopoulos and L. Susskind, Nucl. Phys. **B155**, 237 (1979).

[5] E. Eichten and K. Lane, Phys. Lett. **90B**, 125 (1980).

[6] K. Lane and E. Eichten, Phys. Lett. B **222**, 274 (1989).

[7] R. S. Chivukula, Phys. Rev. Lett. **61**, 2657 (1988); T. Appelquist, T. Takeuchi, M. B. Einhorn, and L. C. R. Wijewardhana, Phys. Lett. B **232**, 211 (1989).

[8] S. Raby, S. Dimopoulos, and L. Susskind, Nucl. Phys. **B169**, 373 (1980).

[9] To make $\alpha_{\rm TC}$ walk we shall take $N_L=6$, implying 6 doublets of quarks, 1 doublet of antiquarks, and 15 doublets of leptons.

[10] T. Appelquist, T. Takeuchi, M. B. Einhorn, and L. C. R. Wijewardhana, Phys. Lett. B **220**, 223 (1989); T. Takeuchi, Phys. Rev. D **40**, 2697 (1989); V. A. Miransky and K. Yamawaki, Mod. Phys. Lett. A **4**, 129 (1989); R. S. Chivukula, A. G. Cohen, and K. Lane, Nucl. Phys. **B343**, 554 (1990).

[11] It is not clear that one can safely ignore excitations of the lowest-lying ρ_T and π_T in walking technicolor models because we really have no good idea of the spectrum of these states. We might expect that they are not serious complications at the low-energy colliders, Tevatron and S$\bar{p}p$S.

[12] There is another type of decay mode of the ρ_8^I which we should mention, namely, $\rho_8^{Ia}\to\mathcal{G}^a\pi_T$, where the π_T is a neutral color singlet or octet. These decays would appear as a resonance in the three-jet invariant-mass distribution. The s-dependent decay rate for this mode has the form $\Gamma(\rho_8^I\to\mathcal{G}\pi_T)=c_T\alpha_{\rm QCD}(s)k^3/s$, where k is the momentum of the gluon. c_T is a constant which we scale naively from the rate for $\rho\to\gamma\pi$, taking into account the color representation of π_T. These decay modes are relevant only for the fairly narrow $\rho_{\bar{D}D}$ that occurs in the Set A masses discussed in Sec. II C. We estimate the total rate to be $\simeq 0.5$ GeV for $M_{\rho_{\bar{D}D}}=225$ GeV. This is considerably less than the several-GeV dijet width we shall find for the $\rho_{\bar{D}D}$ because of the k^3 factor. Therefore, we ignore these (potentially interesting) decay modes throughout the rest of this paper. We thank E. Eichten for reminding us of these decays.

[13] S. Narison, Phys. Rep. **84**, 263 (1982).

[14] M. E. Machacek and M. T. Vaughn, Nucl. Phys. **B222**, 83 (1983).

[15] Choosing the technifermion thresholds at $2\Lambda_i$, rather than the sum of their constituent masses, is consistent with our use of lowest-order chiral perturbation theory.

[16] A. G. Cohen and H. Georgi, Nucl. Phys. **B314**, 7 (1989); U. Mahanta, Phys. Rev. Lett. **62**, 2349 (1989).

[17] T. Appelquist, K. Lane, and U. Mahanta, Phys. Rev. Lett. **61**, 1553 (1988).

[18] We are aware that, if the second-order term in $\beta_{\rm TC}$ is as large as the first-order one, then still higher orders are bound to be important and our calculations of Λ_i are not trustworthy. This is one of the basic difficulties of walking technicolor: in perturbation theory, we cannot know reliably that $\beta_{\rm TC}$ is small for moderately large coupling. We must, therefore, take the pragmatic attitude that the expressions (2.6) and (2.7) *define* an ansatz for $\beta_{\rm TC}$ and proceed accordingly.

[19] We are assuming that Eq. (2.19) is valid despite the sizable weak isospin breaking induced by ETC interactions. See Chivukula *et al.* and Appelquist *et al.* in [10]. In this model, the assumption is probably justified since $F_\pi\simeq F_\psi$ and Λ_ψ is considerably larger than the hard masses of $\psi_{U,D}$.

[20] A. Manohar and H. Georgi, Nucl. Phys. **B234**, 189 (1984); H. Georgi and L. Randall, *ibid.* **B276**, 241 (1986).

[21] Motivated by the additive property of constituent masses in the naive quark model, it seems appropriate to us that hard masses, as well as condensates, should be defined at Λ_i rather than $2\Lambda_i$. For this reason, we assume $\gamma_{m_i}=1$ between Λ_i and $2\Lambda_i$. This makes a factor of 2 difference in the hard masses used to calculate $M_{\pi_T}^2$ and M_{ρ_T}.

[22] In principle, there is another resonant contribution to dijet and technipion production which arises from the direct coupling $\sqrt{2}g_{\rm QCD}^2/g_{\rho_T}f_{abc}\mathcal{G}_\mu^a\mathcal{G}_\nu^b\partial^\mu\rho_8^{0a\nu}$ included by a technicquark loop. However, our approximation includes ρ_8^I only in the s channel. The amplitude from this coupling vanishes because $p_1\cdot\epsilon(p_1,\lambda_1)=p_2\cdot\epsilon(p_2,\lambda_2)=p_1\cdot\epsilon(p_2,\lambda_2)=p_2\cdot\epsilon(p_1,\lambda_1)=0$ when both gluons are in either the initial or the final state. We thank R. S. Chivukula and M. Golden for pointing out this other contribution to us.

[23] See, e.g., CDF Collaboration, P. Giannetti, FERMILAB-Conf-90/85-E (unpublished).

[24] We thank John Huth and other members of the CDF Collaboration for discussions on this and other aspects of the CDF jet data.

[25] The UA2 Collaboration, J. Alitti *et al.*, Z. Phys. C **49**, 17 (1991). We thank F. Pastore for bringing this paper to our attention.

[26] R. S. Chivukula, M. Golden, and E. H. Simmons, Nucl. Phys. **B363**, 83 (1991); (private communication).

[27] M. E. Peskin, Nucl. Phys. **B175**, 197 (1980); J. Preskill, *ibid.* **B177**, 21 (1981).

[28] S. Weinberg, Phys. Rev. Lett. **18**, 507 (1967); C. Bernard, A. Duncan, J. LoSecco, and S. Weinberg, Phys. Rev. D **12**, 792 (1975).

[29] Recently, M. E. Peskin, and T. Takeuchi [Phys. Rev. Lett. **65**, 964 (1990)] have used the same procedure to estimate the contributions from technicolor models to certain precisely measured electroweak parameters. This method should be reliable in old-fashioned models of technicolor, since they are thought to be just scaled-up versions of QCD. For reasons we have touched upon, we doubt that naive scaling from QCD is accurate enough to permit precision electroweak tests in a walking technicolor model. Also, see M. Golden and L. Randall, Nucl. Phys. **B361**, 3 (1991); and B. Holdom and J. Terning, Phys. Lett. B **247**, 88 (1990).